An investigation into multi-component gasoline biofuel droplet and spray using non-ideal vapour-liquid equilibrium models

A THESIS SUBMITTED FOR THE DEGREE OF DOCTOR OF PHILOSOPHY

BY

WAN YANG

Department of Mechanical, Aerospace and Civil Engineering

College of Engineering, Design and Physical Sciences

Brunel University London

March 2021

Abstract

Fuel injection technology plays an important role throughout internal combustion engine development. The mixture preparation inside the combustion chamber affects the combustion process and the pollutant emissions. The formation of particulate matter is difficult to predict. Biofuels are introduced in both gasoline and Diesel engines to reduce combustion emissions. However, biofuels usually behave differently during the mixture preparation process.

The thesis investigates the non-ideal phenomena on evaporation dynamics of multicomponent droplets and spray. The UNIFAC model has been implemented into the software to determine the activity coefficients that affect the evaporation process and mixture distribution inside the combustion chamber. The results demonstrate good agreement with existing measurement and numerical data. For the model validation, the E36 and E78 have been studied. Raoult's law can reasonably approximate the evaporation process of the E36 mixture. However, the non-ideal Vapour-liquid equilibrium (VLE) model must be used to predict the evaporation of the E78 mixture properly. The evaporation dynamics of a four-component gasoline/ethanol spray was finally investigated. A ternary mixture surrogate composed of iso-octane, n-pentane, and n-decane has been used to provide a more realistic engine spray simulation. The Poynting factor is also introduced to give a more detailed non-ideal VLE model. The simulation results demonstrate that high ambient pressure significantly impacts the liquid evaporation process. The non-ideal evaporation model significantly affects the vapour composition during evaporation, which determines spray combustion and emission dynamics.

Compared to other liquid activity coefficient models. The UNIFAC shows unique advantages for its simplicity. The model only requires properties of constituent functional groups of each liquid component. The requirement can be useful when there is no VLE data available for binary-component subsystems of the multicomponent mixture.

Acknowledgements

I would like to thank:

My supervisor Dr. Jun Xia for his guidance and support during the last 5 years.

Former and current students Dr Yizhi shao, Mr. Enshen lv for putting up with sharing idea and providing intellectual stimulation for four years.

My late parents, Jinli and Junyong, for raising me and supporting my PhD study in the last 29 years.

Table of Content

List of Figures

List of Publications

W.Yang, J. Xia, X.Y. Wang, K.D. Wan, A. Megaritis, H. Zhao, Predicting evaporation dynamics of a multicomponent gasoline/ethanol droplet and spray using non-ideal vapour-liquid equilibrium models. International Journal of Heat and Mass Transfer 168 (2021) 120876.

Abbreviation

ODE	Ordinary Differential Equation
CFD	Computational Fluid Dynamics
RANS	Reynolds-averaged Navier-Stokes
LES	Large Eddy Simulation
VLE	Vapour-Liquid Equilibrium
NRTL	Non-Random two liquids
UNIFAC	UNIQUAC Functional-group Activity Coefficients
UNIQUAC	Universal Quasichemical
GDI	Gasoline Direct Injection
PM	Particulate Matter
PFI	Port Fuel Injection
KHRT	Kelvin-Helmholtz Rayleigh-Taylor
TAB	Taylor analogy breakup

Nomenclature

We	Weber Number
ρ_l	Liquid density
Oh	Ohnesorge number
v	Liquid velocity
ρ_d	Droplet density
σ	Surface tension
μ_l	Liquid Dynamic Viscosity
l	Characteristic Length scale

r_d	Droplet Radius
C_D	Droplet Drag coefficient
Re, Re_d	Droplet Reynolds number
B_m	Spalding mass number
B_T	Spalding heat number
L_{eff}	Liquid phase latent heat
$Y_{F,s}$	Fuel mass fraction at the droplet surface
$Y_{F,\infty}$	Fuel mass fraction at ambient gaseous phase
T_∞ T_g	Ambient temperature
T_s	Droplet Surface temperature
ρ_g	Density of ambient gas
D, $D_{i,m}$	Mass diffusivity
Nu'	Corrected Nusselt number
h	Convective heat transfer coefficient
k , k_g	Thermal conductivity of the gaseous phase
Pr	Prandtl number
d_d	Droplet diameter
$\dot{m}_{diff}$	Enhanced diffusive mass flux
Sh_{AB}	Altered Sherwood number
$\dot{m}$	Droplet evaporation rate
Bi	Biot number
h_{vap}	Droplet Latent heat
vap	Vapour
T_d	Droplet Temperature
U_{dmax}	Maximum droplet velocity
C_F	The friction coefficient of the evaporating droplet

χ Enhanced factor (Enhancement to liquid thermal conductivity or liquid diffusion)

δ Liquid Thermal boundary layer thickness

ε_i Evaporative flux fraction of component i

$B_{m.i}$ Spalding mass of component i

$\dot{m}_\iota$ Evaporation rate of component i

Le Lewis number

$c_{p,v}$ Vapour-phase (fuel) specific heat

$c_{p,g}$ Gaseous-phase specific heat

$h_{vap,i}$ Latent heat of component i

c_d Droplet heat capacity

x_i^v Vapour mole fraction of component i

f_i^L liquid phase fugacity

f_i^v Vapour phase fugacity

φ_i^v, φ_i^L Vapour and Liquid phase Fugacity coefficient

p Ambient pressure

$P_{sat,i}$ Saturated Vapour pressure

V_i^L Molar liquid volume

γ_i The activity coefficient of the liquid phase

x_i^L Liquid mole fraction of component i

γ_i^C Combinatorial activity coefficient in the UNIFAC model

γ_i^R Residual activity coefficient in the UNIFAC model

θ_i Area fraction of functional group i

Φ_i Segment fraction of functional group i

$v_k^{(i)}$ Number of occurrences of the functional group i

Ψ_{mn} Group interaction parameter (m and n stands for different main groups)

p_{tot} Total vapour pressure

T_{ref} Reference temperature used in the DPM model

Y_{ref} Reference mass fraction used in the DPM model

α_Y Averaging coefficient for T_{ref} and Y_{ref}

m_d droplet mass

$\overrightarrow{u_p}$ Droplet velocity

$\vec{u}$ gaseous phase velocity

r radius of a newly formed droplet caused by the breakup

Ta Taylor number

τ Droplet breakup time by using the KH model

Ω Maximum growth rate for the KH model

K_{RT} The wavenumber for the RT model

τ_{RT} Breakup time for the RT model

r_c Child droplet radius calculated by the RT model

S_m Mass source term caused by evaporation or chemical reaction

$\vec{F}$ Additional force, i.e. Gravity.

h sensible enthalpy

NP Number of Particles

$\dot{m}_s$ The mass flow rate of the liquid phase

ϑ Spray Cone angle

$m_{d,0}$ Initial droplet mass

α_{ij} Separation factor

Chapter 1. Introduction

1.1 Research Background

Fossil fuels combustion is commonly applied in generating electricity, heat and kinetic energy. Fossil fuel will remain dominant in the global energy mix despite developing different kinds of renewable energy such as wind, solar energy etc. Further, fossil fuels' total power will increase based on the rising population and GDP growth. Therefore, the combustion of fossil fuels still plays an essential role in energy supplies in future.

Liquid fuels are widely used in internal combustion (IC) engines and gas turbines that have been well developed in the past decades with the increasing demand for public transport and global trading. Liquid fuels have a high energy density that ensures the development of a compact combustion device. They are unlikely to be replaced by many other energy supply functions due to their significant advantage and benefit in long-distance transport. However, companies and researchers' substitution with biofuels are developing to implement more emission regulations on IC engines. The biofuel derived from biomass helps reduce greenhouse gas and carbon dioxide, and it is one kind of renewable energy and easier to produce. Gasoline mixed with ethanol is widely adopted globally; it is commonly used in America and Germany. E85 fuel with 85% ethanol by volume is famous in racing competition due to its anti-knock value and low costs. Based on the IEA prediction [2], biofuels share will reach up to 27% of the total fuel consumed in transportation in 2050.

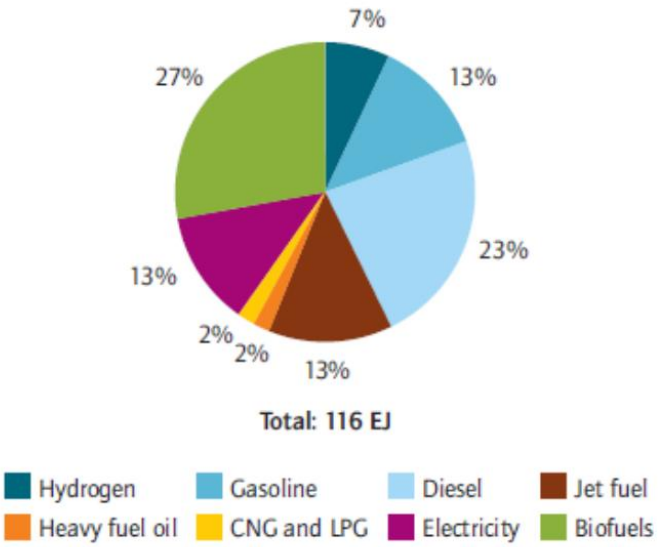

Figure 1. 1 2050 Global energy share in the transport sector [2]

1.1.1 GDI Engine

The fuel is delivered straight into the engine cylinder in a Gasoline direct injection engine, which offers increased thermal efficiency than traditional port fuel injection spark-ignition engines. The evaporative cooling of the air charge with the new injection method ensures a higher compression ratio as the in-cylinder fuel evaporation process lowers the cylinder temperature. The difference between a Port fuel injection gasoline engine and a GDI gasoline engine is shown in Figure 1.2. Compared to a GDI engine, the injection takes part in the intake stage. The fuel and air are already partially premixed before being injected into the cylinder. A liquid film may form on the intake pipe that deteriorates the overall injection control. In general, a GDI engine has two operating modes: The homogeneous mode is available when the early injection is applied. The evaporation of the liquid fuel reduces the charge temperature that allows higher volumetric efficiency. The stratified mode happens when the rich

ignitable mixture is near the spark plug. The stratified charge can reduce the engine pumping loss during operation. The stratified charge gives little time for the form of the homogeneous mixture inside the cylinder, leading to a higher particular matter (PM) and unburnt hydrocarbon emissions.

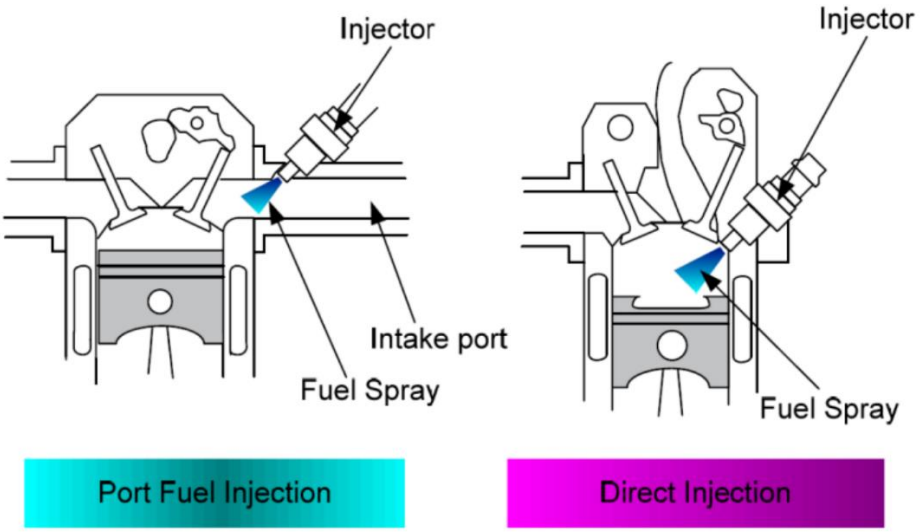

Figure 1.2. Port Fuel injection vs Direct injection.

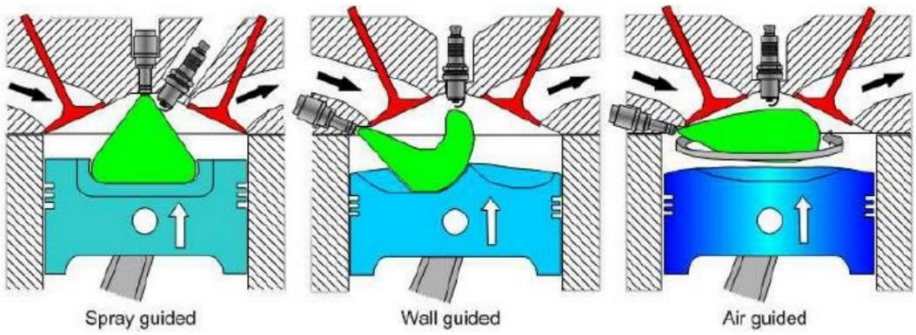

Figure 1.3. Different types of GDI engines

Figure 1.3 demonstrates the mainstream of the GDI engines used in production cars. The wall-guided method is the first modern GDI engine that ensures higher engine efficiency. A spray-guided GDI engine has the highest efficiency in theory as the fuel is injected into the area near the spark plug and evaporated results in less bowl and wall wetting. However,

the fuel may easily form a liquid film on the bowl or cylinder wall resulting in a higher PM emission during combustion.

It is crucial to understand the combustion process in a GDI engine as the fuel and air are no longer premixed or homogeneous under a stratified charge operating condition. The spark ignition may be triggered when the liquid spray is still not fully vapourised. Therefore, a more in-depth study is necessary to develop GDI engines.

1.1.2 Spray evaporation

The spray studies play a crucial role in developing an internal combustion engine. The vapourisation of liquid fuels involves the fuel breaking up into finer ligaments and droplets, leading to a fast evaporation and oxidiser mixing process. Many research institutes widely study the internal combustion engine sprays, and detailed experimental data has been produced and published throughout the decades. Spray analysis has advanced to a stage when the improved understanding of a spray process's respective phases, including internal-injector flow, spray atomisation, spray and droplet evaporation, fuel/air mixing, ignition, combustion and emissions, has been achieved using advanced measurement and simulation techniques. However, an integrated simulation tool is still much needed to save the cost of design and optimisation of liquid-fuel injection processes.

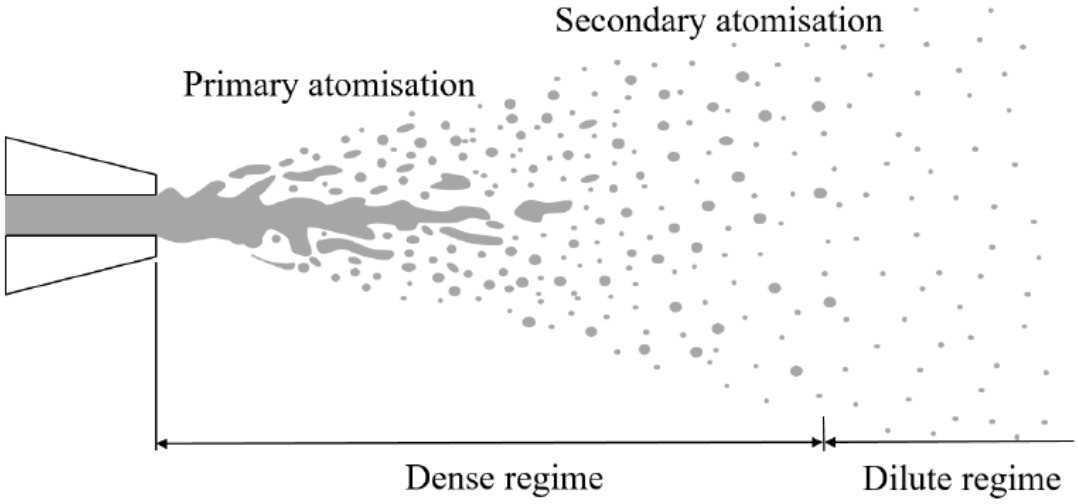

Figure 1.4. Spray atomisation process

Biofuel mixed with gasoline improves fuel efficiency and meet the new engine regulations. Correctly modelling multi-component spray evaporation becomes essential since a biofuel mixture usually consists of alkanes, alcohols and dimethyl, distinctly different in chemical structure molecular size. The structurally dissimilar components behave rather differently during the evaporation process, and structural interaction inside the mixture that affects evaporation cannot be ignored. Further, gasoline and diesel consist of multiple components with a significant molecular dissimilarity. The different fuel component behaves differently based on various operating conditions. Figure 1.5. demonstrates a typical representative sample of diesel fuel includes iso-alkanes, n-alkanes, cycloalkanes, etc. Here, alkylbenzenes are benzene derivatives, a subset of aromatic hydrocarbons. The non-ideal behaviour may become significant when aromatic hydrocarbons are mixed with paraffin [71].

The modelling approaches used in many spray calculations have assumed a single-component fuel with lumped properties. Although this assumption has been convenient numerically, a single-component fuel's

distillation behaviour is different from actual gasoline and diesel. Therefore, a single-component surrogate could misinterpret the vaporisation process under many engine operating conditions. Insufficient evaporation models may limit the precision of the simulation and lead to unrealistic results.

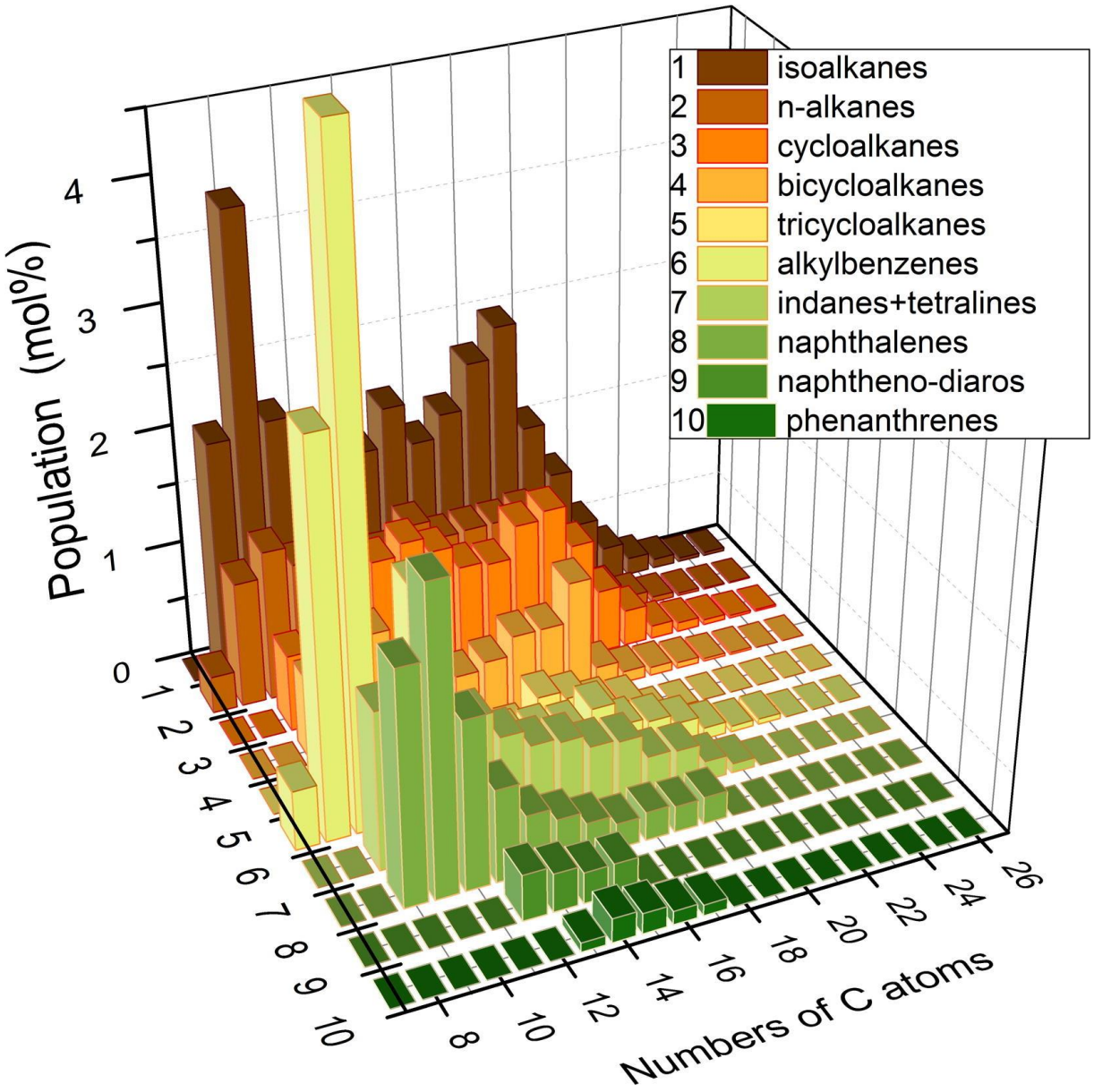

Figure 1.5. The distribution function of various hydrocarbons versus the numbers of carbon atoms in a representative sample of diesel fuel provided by Sazhin et al. [71]

It is difficult to capture every detailed evaporation and combustion process in a simplified combustor or an actual IC engine. The biofuel liquid penetration and component's vapour distribution inside the cylinder provides promising engineering design information. The numerical simulations on biofuel sprays are not widely studied. Therefore, there is a need for a computational tool that can precisely provide the behaviour of the complex evaporation process confronted with the above experimental bottleneck.

1.1.3 Limitation for current numerical models on Vapour-Liquid-equilibrium

Vapour liquid equilibrium (VLE) determines the vapour concentration of each component on the droplet surface. The ideal VLE law only considers the vapour pressure of each component, whereas the non-ideal VLE law considers the internal molecular force of each component. Wilson, Non-random-two-liquids (NRTL), and UNIFAC models are widely used to calculate the VLE in chemical engineering. Compared with Wilson, UNIFAC and NRTL provide more accurate results [4,5]. However, NRTL requires experimental VLE data of all binary-component subsystems of a multicomponent mixture to obtain the complete VLE diagram. The UNIFAC model is an alternative when the experimental data are not available for completing the NRTL model. When more than two components are in the system, the UNIFAC model is easier to use as it divides the components into functional groups. And all functional groups are already obtained [5]. In addition, the UNIFAC model may perform better than the NRTL model for aqueous alkanolamine solutions [6].

1.2 Numerical simulation for engine development

1.2.1 Models for Turbulence

The three main approaches to model the turbulent motion are: Direct numerical simulation (DNS), Large-eddy simulation (LES), and Reynolds-Averaged Navier-Stokes (RANS). DNS has the highest computational cost as it does not require any turbulence model. It requires a fine enough mesh to resolve all the flow motion. LES assumes several eddies scale characterize the turbulent flows, and the Navier-stokes equations resolve the eddies larger than the mesh scale. The turbulence sub-models solve the smaller eddies. RANS model has been widely used to solve the engineering problem, the model ensemble a range of turbulent fluctuation rather than a specific eddy variation. Therefore, RANS provides a fast simulation process with a low computational cost.

1.2.2 Models for Spray simulation

Spray modelling is fundamental for engine simulation since it directly affects combustion processes and emissions. To simulate the interaction between liquid and air is a difficult task, and the simulation models are still under heavy development. Figure 1.4 demonstrates a typical atomization process of an engine spray. The process can be classified into primary breakup and secondary breakup. Initially, a liquid core exists at the nozzle exit, and during the primary breakup, the liquid core separates into large ligaments near the nozzle. Finally, small droplets distribute in the dilute regime during the secondary breakup. Figure 1.6 demonstrates a typical gasoline engine spray.

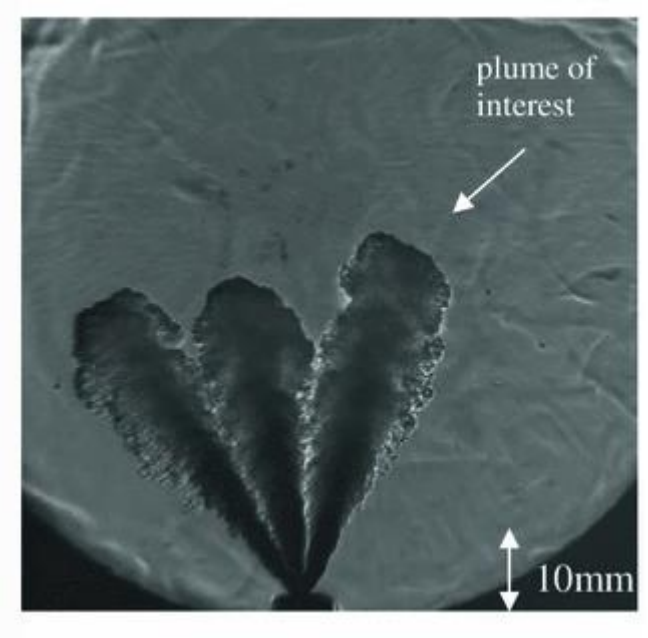

Figure 1.6. Gasoline engine spray [27]

There are three numerical approaches to model the liquid phase, namely, Volume Of Fluid (VOF), Eulerian, and Discrete phase model (DPM) / Discrete droplet model (DDM). Here, VOF tracks the interface between the liquid and gas phases. The model provides an accurate liquid-gas interaction development. The model obtains the shapes of all liquid ligaments and droplets. In the Eulerian approach, Both liquid and gaseous phases are modelled as the continuous phase. Both phases are solved using the ensemble averaging method. However, the computational cost is the highest among the three models as a much more refined mesh is required to capture the ligament and droplet distribution.

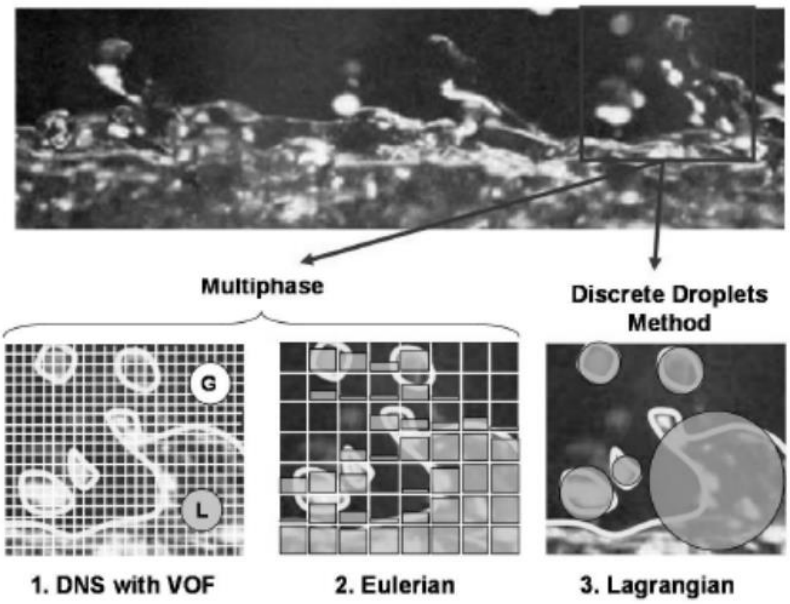

Figure 1.7. Different numerical approaches for spray simulation [72]

The DPM method, also known as the Lagrangian approach, is illustrated in Figure 1.7. The model simplifies the near nozzle liquid motion to large droplets, and the droplets are tracked in a Lagrangian framework. Therefore, the 3-D liquid phase is simplified into a zero-dimensional liquid parcel point. The model is widely used in engine spray simulation in both industry and academia as it provides a reasonable result with the lowest computational cost. However, the simplification ignores the initial turbulence at the liquid phase near the nozzle exit. The results are normally inaccurate at the dense liquid region as the unstructured liquid ligaments are assumed to be large liquid droplets. Bernoulli's equation calculates the initial droplet injection velocity and mass flow rate.

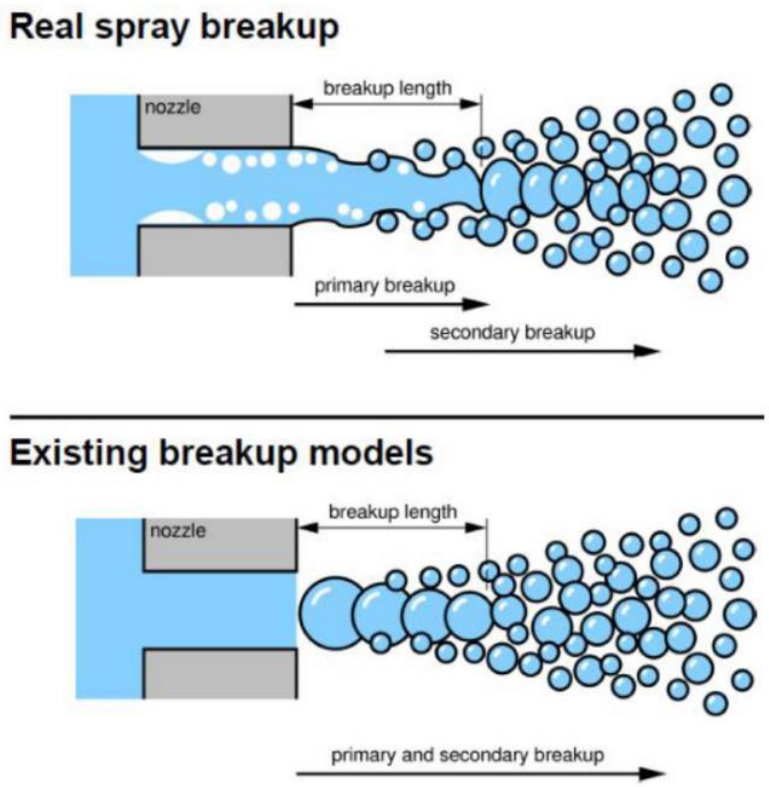

Figure 1.8. DPM / Lagrangian method provided by Vectis [33]

A coupled method between VOF and DPM is introduced to overcome the limitation of both models. The Coupled approach can simulate the dilute zone and the dense zone of the spray atomization process. In general, The VOF method is accurate in simulating the complex behaviour of the dispersed multiphase flow. When large ligaments break up into small droplets in a dilute regime, the gas-liquid interface becomes difficult to track as the droplets require a finer spatial resolution. The coupled approach significantly reduces the computational cost, and it has great potential for realistic scale spray simulations.

1.3 Strategy

This thesis describes the numerical simulation on multicomponent droplets and sprays evaporation under gasoline engine operating conditions. The Euler-Lagrangian simulation model is adopted to model the two-phase flow throughout the thesis. The model represents the flows with a finely dispersed liquid phase. The Eulerian framework accounts for the solution of the continuous gaseous phase. In contrast, the Lagrangian framework is applied to simulate and track the dispersed liquid phase that assumes a point particle in the numerical domain. In spray simulations, the continuous phase's turbulent flow field is solved with the Reynolds-Average Navier-Stokes (RANS) approach.

The non-ideal effect needs to be considered, and the UNIFAC model will be implemented into the commercial software package ANSYS.

1.4 Objectives

The present work focuses on the simulation of the multi-component droplet evaporation process. The objectives of this thesis are:

Implement a more realistic droplet evaporation model (UNIFAC) that considers the non-ideal effect of molecular dissimilarity for more précised simulation results.

To investigate the non-ideality phenomena that exist in a biofuel droplet.

To investigate and demonstrate the effect of the non-ideality impact on spray simulation.

The extension of the model used towards modelling the evaporation of a many-component liquid mixture is studied to demonstrate the necessity of using the more realistic evaporation model.

1.5 Thesis outline

This thesis is structured into four main sections across five chapters. The first chapter presents the introduction, objectives, and research background information.

Chapter 2 presents the experimental and numerical research on multicomponent droplet and spray that has been done in the past.

Chapter 3 provides the fundamental research methodology for modelling multi-component spray and single droplet simulation.

Chapter 4 presents the simulation results with validation for a bi-component single droplet. The simulation is based on the different ambient conditions to evaluate the impact of the non-ideality effect.

Chapter 5 presents the 3-D simulation results from a single spray plume under an actual engine operating condition.

Chapter 6 summarises the results from chapters 3, 4 and provides the recommended works that arose from the project

Chapter 2 Literature review

2.1 Experimental study for Droplet evaporation

Most of the studies on droplet evaporation are focused on single-component droplets. The research only provides the results of the radius regression with evaporation lifetime and the droplet temperature history. Besides, the measurement technique may alter the droplet's shape and heat transfer process.

The historical development of the experimental study began with the investigations on a pure-component droplet and further developed into multicomponent droplets.

Frössling [8] provides the fundamental studies on droplets evaporation based on a dimensionless analysis. The relationship for the Sherwood number (Sh) is defined as a function of the Reynolds (Re) and Schmidt number (Sc). The evaporation process droplet was carried out at room temperature with Reynolds numbers ranging from 2 [-] to 800 [-], and the droplet diameter was set from 0.1 to 0.9 [mm].

Ranz and Marshall [9] conducted the experiments on water droplets with a Reynolds number range from 0 to 200 [-]. The droplet diameters are defined from 0.6 to 1.1 [mm]. A microfilm viewer measured the droplet diameter. The experiment results were used to modify the coefficient of Frössling's relationship.

Beard et al. [10] measured small water droplets evaporating in a wind tunnel with the initial size ranging from 70 to 375 [μm]. The experimental

results further refined the numerical model. The Sherwood number can be applied to 2 ($Sh = 2$) when the Reynolds number is less than 2 [-].

The levitation techniques were often applied to study droplet evaporation;

For acoustic levitation, An acoustic field levitates the liquid droplet. The flow around the droplet under high-pressure gradients usually affects the droplet's evaporation behaviour. Further, the droplet size was difficult to obtain as the droplet shape was distorted during evaporation.

Brenn et al. [73] presented the results from droplets containing 3 to 5 components. In their research, alcohols are selected to represent organic compounds. The mixing of the substances leads to a deviation from the ideal liquid mixture behaviour due to the dipole moment of the hydroxyl group. The non-ideal effect caused by the dipole moment is calculated by both Wilson and UNIFAC VLE law. The numerical model developed by Sirignano et al. was applied to compare their experimental data. The results demonstrated a good agreement on droplet diameter regression (normalized squared droplet diameter [-] vs droplet lifetime [s]). Their works validated the widely used 0-D evaporation model on multicomponent evaporation.

Tuckermann et al. [74] also used the acoustic levitation method like Brenn et al. Different n-alkanes were investigated, and the droplet surface histories and evaporation rates were presented. Further, they also raised the droplet temperature history by using IR thermography.

The optical levitation uses radiation pressure forces to stabilize the droplet. The droplet must not absorb the light to avoid the additional heat generated by using this method. The initial droplet size should be small enough to be levitated with reasonable laser power.

Roth and Frohn [75] studied droplet surface histories of the bi-component droplet with different initial compositions at room temperature.

Droplet suspension techniques are still widely adopted in experimental studies due to the simplicity of the method. Here, a thermocouple is used for the droplet suspension. The heat transfer through the support fibre was studied and presented by Nomura et al. The initial droplet size should be above one millimetre to ensure the droplet diameter is much larger than the fibre. The larger droplet size provides a longer evaporation lifetime so that the researcher can obtain a detailed size history.

The pure decane, heptane, and decane/heptane mixture have been studied by A.Daïf et al. compared with the numerical model created by Abramzon and Sirignano [7]. The droplet in their study was suspended on a permanent holder to prevent the droplet from free-falling, and convective vapourisation was considered. The comparison validated the 0-D droplet model provides a decent simulation result on droplet radius regression and surface temperature history.

The fuels are multicomponent. In addition to droplet size and lifetime, temperature and composition are important in biofuel or real fuel evaporation studies. Thermocouples can obtain the droplet temperature when a droplet is suspended on the wire. However, the droplet should have a diameter of two millimetres. The infrared thermography has been applied by Daif et al. [7]

The droplet composition can be measured by rainbow refractometry. However, this method can only be used for bi-component droplets. Raman scattering can be adopted for determining the droplet composition for single optically levitated droplets.

Unfortunately, very few studies consider the mixture composition results for a multi-component droplet. The majority of the studies were based on a droplet larger than one millimetre so that the deformation and internal heat transfer process may significantly affect the experimental results.

2.2 Experimental study multi-component biofuel spray vapourisation

The conventional gasoline fuel has various components and has often been simplified by using surrogates like iso-octane, n-hexane, etc.

The gasoline combustion process is increasingly controlled by direct injection technology. Recently, Biofuels are increasingly being blended into conventional gasoline to meet the emission regulations. The complex mechanisms remain unclear. Therefore, many researchers have been seeking solutions by conducting multi-component spray experiments.

T. Knorsch et al.[76] studied the evaporation process of biofuel sprays in Direct injection spark-ignition (DISI) engines. The spray measurements were carried out using an optically accessible spray chamber. A six-hole solenoid injector generated the spray plume. The local droplet size and spray propagation were studied in the chamber. A variety of single-component fuels and mixtures were tested at different ambient conditions to identify the most significant fuel properties and evaporation rate.

P.Keller et al. [4] used experimental and numerical methods to analyze the iso-octane/ethanol spray by using T.Knorsch' experimental setup. The experimental results provide both liquid and vapour penetration of one of six spray plumes. The simulation with two VLE models (Raoult's and

NRTL) demonstrates a significant difference in component concentration's continuous (gaseous) phase. In contrast, the model does not significantly affect the liquid and vapour penetration length.

M. Andersson et al. [77] studied a hollow-cone spray using a gasoline-like multi-component model fuel blended with ethanol. For the gasoline surrogate, the light components evaporate much faster than other heavy components at 363K; the difference became the components became smaller as the temperature was raised. The evaporation of ethanol-based fuels is much slower at a lower temperature.

2.3 Numerical study on single droplet evaporation

The vapourisation models, including droplet heating, evaporation, and boiling, simulate the heat and mass transfer process between the liquid and gaseous phases. The vapourisation and heating process takes part as the liquid is injected into the chamber, and it is crucial to the final combustion and pollutant formation process. S. Sazhin et al. demonstrated the importance of thermodynamic models' importance in predicting multi-component droplet evaporation [78]. The vapour-liquid equilibrium model also plays a vital role in modelling the multicomponent evaporation and boiling process.

Researchers are keen to develop a robust model to accurately simulate the droplet’s behaviour—four different models for solving the liquid phase droplet evaporation.

Table 2.1 presents the evaporation model for solving single droplet evaporation.

0D	1D
Constant-droplet-temperature model	The finite thermal conductivity model
Rapid mixing model (infinite-liquid-conductivity)	Internal mixing model

Table 2.1 Single droplet evaporation model

Here, the constant-droplet-temperature model is also known as the d^2-law model. The model was widely used to study the evaporation process of a single droplet [78] as the gas phase was supposed to be quasi-steady, and droplet temperature does not vary during the evaporation process. An infinite-liquid-conductivity model, also known as the Rapid mixing model, assumes a uniform temperature of the liquid, but the droplet temperature is time-dependent. It has been studied that the internal droplet temperature may not be uniform if the gas-to-liquid thermal capacity ratio is smaller than 0.3. A spherically symmetric transient droplet-heating model (or finite conductivity model) provides the internal droplet temperature gradient. However, the computational cost is significantly increased. An effective conductivity model accounts for internal circulation and internal convective heating inside the droplet. The model always applies with the 1-D conduction-limit model as the internal circulation has no impact on heating when droplet temperature is uniform. It is essential to know that all the vaporisation models introduced are used to model the droplet's evaporation. The gas phase is under a quasi-steady state throughout the evaporation because the thermal diffusivity in the gas phase is much larger than the liquid phase. The internal mixing model is

applied when the droplet is a mixture. It not only has a temperature gradient inside the droplet but also has a species gradient.

2.3.1 Multicomponent droplet and spray simulation

A single component surrogate cannot accurately capture the injected fuel's detailed vaporisation process. Therefore, developing the surrogate and vaporisation model for the spray behaviour in-depth study is necessary.

In a multicomponent liquid, different components vaporize at different rates. Component's mass diffusivity is generally smaller than each component’s thermal diffusivity result in a faster vaporization speed of a more volatile substance. The phenomena require a more complex solution that includes a liquid-phase continuity equation, a phase-equilibrium model, and the gaseous phase multicomponent species continuity equation.

Sirignano declared that the characteristic time for the liquid-phase mass diffusion based on the droplet radius is longer than the droplet lifetime. Therefore, most multi-component spray research ignores the liquid mass diffusivity effect to reduce the model's complexity and, consequently, reduce the computational cost.

2.3.1.1 Ideal mixture in multicomponent droplet simulation

For most gasoline surrogates, the fuel can be assumed to be ideal, where the vapour-liquid equilibrium can be directly defined using component vapour pressure.

T. Kitano et al. studied the fuel droplet evaporation and combustion process under different ambient pressure, temperature conditions [31]. The effect of natural convection is considered and becomes significant with increasing ambient pressure. As the ambient pressure increases, the droplet evaporation is suppressed by a higher boiling temperature. However, the lower latent heat and greater droplet surface area caused by thermal expansion increase the evaporation rate. They further apply the simulation on a two-component simulation that includes n-decane, 1,2,4-trimethyl-benzene, and a three-component simulation that includes n-dodecane, iso-octane, and toluene [32].

Zhang et al. [15] used a probability density function (PDF) to represent the fuel's molecular weight distribution. The PDF function is a continuous thermodynamics approach, significantly reducing the computational time compared with the discrete method. The Vapor-liquid equilibrium and vapour-phase transport equations are calculated based on the molecular weight of each component and the PDF method's boiling temperature. However, the model ignores the mixture's molecular dissimilarity, leading to a noticeable difference in the simulation result. However, the continuous thermodynamics approach model cannot be coupled with the detailed multi-component chemistry. Also, the model cannot simulate the property difference between Isomers.

X. Ren et al. [17] used a continuous thermodynamics based evaporation model to simulate the diesel spray evaporation process. The fast evaporation of the light-end components enhanced the evaporation rate, and the droplet lifetime was significantly reduced. A significant difference

in the droplet lifetime is observed using both the single component and multi-component surrogates. The soot formation calculated by the multicomponent result agrees with the experimental data.

Yongchul Ra and Rolf D. Reitz [16] introduced a multi-component spray modelling vaporisation model. The model considers both evaporation and boiling process as the droplets are more frequently in the boiling situation under practical engine operating conditions. Their model considers the internal heat transfer as the conventional evaporation models assume the 0-gradient unity temperature throughout the droplet, which leads to over-estimation or under-estimation of the droplet's evaporation rate. Besides, the VLE model applies Raoult's law to calculate the vapour mole fraction at the droplet surface. The results indicate that the local vapour phase's component distribution differs significantly from a single-component surrogate simulation. Besides, both simulation for diesel and gasoline spray proves that the light-end components evaporate faster and always appear upstream of the spray vapour plume. In contrast, the heavy components are usually located near the tip of the spray.

P. Yi et al. [20] used a hybrid multicomponent vapourisation model to simulate the surrogate. The HMC separates the fuels into several discrete classes, which allows a more detailed description of the fuel. The HMC model has demonstrated a much higher computational accuracy compared with the CMC and DMC model. [21-22] However, the diffusion coefficients are assumed to be the same for all hydrocarbon classes in reference. [21, 22] V. Ebrahimian et al. implemented the diffusion coefficient Hirschfelder's law into the HMC model as the assumption may lead to the error estimation of the enthalpy diffusion [23]. The results from the HMC model shows a more accurate estimate compared with a reduced DMC model and CMC model.

The HMC model can reproduce the species with similar molecular weight in different hydrocarbon classes. In contrast, the full DMC better forecasts with the experimental data. Therefore, the improved HMC model can reduce the computational cost compared with a complete DMC model but still offer a decent estimation.

2.3.1.2 non-ideal liquid in multicomponent droplet simulation

The non-ideal effect on phase equilibrium should also be considered. The constituents of a solution are normally intimately intermixed, and the partial properties cannot vary independently as molecular interactions affect each component's properties in the mixture [1]. Raoult's law is a simplified method for calculating Vapour-liquid equilibrium and is widely used in research studies. The law assumes that each component's partial vapour pressure is self-independent and can only provide reasonable solution behaviour when the molecular species are not too different in size and have the same chemical nature. When actual vapour concentrations cannot demonstrate linear relations for a solution's behaviour, the activity coefficients are used to express Raoult's law's deviations [4, 16, 27]. The coefficient can be obtained directly from experimental data and then be fit into mathematical models.

Ju et al. [12] used the UNIFAC VLE model to demonstrate the significant non-ideal effect in dimethyl ether (DME)/n-heptane mixture. The simulation considers both the non-equilibrium evaporation and the non-ideal impact of the VLE. The non-equilibrium model ensures the mass diffusion for each component inside the droplet, and the internal

composition varies throughout the evaporation time. Besides, the simulation ignores the nucleation effect of the droplet caused by boiling as the simulation only considers small droplets ($d_d \leq 50\mu m$). The simulation tested the evaporation process of the bi-component droplet under different temperatures and ambient pressures.

Based on the simulation [12], Ju et al. [13] further studied the bi-component droplet by focusing on different initial droplet diameters. The decreased initial droplet diameter reduced the evaporation rate of both components in the mixture. The simulation results also prove that the ambient pressure does not significantly impact the droplet lifetime of the 25DME droplet (25% dimethyl ether by a mass fraction). However, higher ambient pressure can increase the peak evaporation rate of DME.

S. Sukumaran [18] used a multicomponent evaporation model provided by Sirignano to simulate a 5-component bio-diesel surrogate spray combustion. The results demonstrate a similar trend with the experimental data, and the model enhanced the understanding of the evaporation process of multicomponent bio-diesel fuels.

P. Keller et al. [3, 4, 27] firstly apply the one-way coupling method based on a lumped (0-D) evaporation model introduced in [8] to simulate a single iso-octane ethanol droplet [3]. The linear mixing rule is applied to the iso-octane/ethanol mixture. A more accurate non-ideal non-random two liquids (NRTL) model validated with experimental data presented by Wen et al. [19] is used to calculate the vapour-liquid equilibrium. The non-ideal model affects the droplet temperature and the evaporation rate of each component significantly. A separation factor for component relative volatility is introduced to enhance the understanding of the phenomena. The VLE model was also applied with the spray simulation validated with experimental data presented in [4, 27].

S.Sazhin et al. [71] developed a Multi-dimensional quasi-discrete model to simplify diesel fuel droplets components to a smaller number of components, and the model was a step forward in the development of a model for complex multi-component evaporation simulation. However, the model assumes the diffusion coefficient of all species is the same and the assumption introduces errors that are impossible to quantify.

2.4 Summery

In this chapter, a literature review of both experimental study and numerical study on multi-component droplet/spray evaporation has been presented. The literature indicates that the rapid mixing model with a detailed vapour-liquid equilibrium can achieve accurate results compared with experimental studies. However, the non-ideal effect during spray evaporation is not well understood, and the empirical research on multicomponent droplet evaporation is still very limited. The numerical study on non-ideal mixture demonstrates the importance of correctly modelling the fuel's physical properties.

Chapter 3. Methodology

3.1 Numerical Model for Droplet evaporation simulation

There are three major approaches for calculating droplet temperature in a simplified droplet and spray evaporation modelling: Zero-, quasi-, and one-dimensional vaporization models. The heat transfer model determines the droplet surface temperature, which is crucial in modelling the droplet evaporation rate as the Spalding mass is based on droplet surface temperature. In single-component gasoline/diesel spray simulation, the droplets are assumed with infinity conductivity, which means the droplet will rise to its wet-bulb temperature with no temperature gradient inside.

The droplet lifetime of a single component in a stagnant gas has been studied for decades. The numerical model assumes that the droplet temperature remains uniform during evaporation and ignores the droplet surface and internal motion. The radiation heating of the droplet and combustion on the droplet surface are also ignored. Therefore, the conservation equation for species and energy in the gaseous phase around the droplet can be solved by considering two different species: nitrogen (or air) and fuel.

Like the continuous phase, the governing equations describing the droplet's evaporation can be introduced by solving mass, momentum, and heat equations. We shall first present the mass equation to calculate the droplet evaporation rate, then the heat equation for calculating the energy been absorbed by the droplet.

The equation for describing the evaporation rate can be calculated as:

$$\dot{m} = \frac{dm}{dt} = 2\pi d_d \frac{\lambda}{C_p} \ln(1 + B_T) = 2\pi d_d \rho_g D_{i,m} ln(1 + B_m) \qquad (3-1)$$

Where d is the current droplet diameter and the C_p is the specific heat capacity of the evaporating fuel component. The Spalding mass B_m [-] can be calculated as:

$$B_m = \frac{Y_{F,s} - Y_{F,\infty}}{1 - Y_{F,s}}, B_T = \frac{C_{pF}(T_\infty - T_s)}{L_{eff}} \qquad (3-2)$$

with $Y_{F,s}$ denotes the fuel vapour mass fraction at the droplet surface and $Y_{F,\infty}$ is the fuel vapour mass fraction at an infinite far field in the ambient gas phase. The value $Y_{F,\infty}$ is set to zero in a Single droplet simulation. and L_{eff} is a useful enthalpy of vaporisation for the fuel species given by

$$L_{eff} = L + \frac{\dot{Q}_L}{\dot{m}} \qquad (3-3)$$

in which the heat transferred from the droplet surface towards the droplet interior is $\dot{Q}_L$. Under steady-state conditions, the temperature is uniform, and therefore no heat conducts inwards from the droplet surface, thus $\dot{Q}_L = 0$ and $L_{eff} = L$.

We assume that the no ambient gas will dissolve into the droplet, and when the droplet temperature is below the liquid boiling point, the surface will reach equilibrium and therefore, the vapour mole fraction $X_{F,s}$ can be calculated using the saturated vapour pressure of the fuel component and the ambient pressure, $X_{F,s} = \frac{P_{vap}}{P}$ .Finally, the mass fraction of fuel at the droplet surface can be converted from mole fraction $X_{F,s}$ using the fuel and air molar masses.

By assuming the constant droplet temperature at a steady-state, the d^2-law is formed in equation (3-4)

$$\frac{dd^2}{dt} = -\frac{8\rho_g D ln(1+B_m)}{\rho_d} \qquad (3-4)$$

During spray injections, droplets have high velocity due to high injection pressures that lead to convective enhancement of heat and mass transfer between the ambient gases and droplet surface. The Nusselt number Nu and Sherwood number Sh for heat and mass diffusion are equal to 2 when the convection term does not exist. But the Stefan convection does exit as the spherical droplet start to evaporate.

$$Sh_{AB} = \frac{k_c d_d}{D_{i,m}} = 2 + 0.6 Re_d^{\frac{1}{2}} Sc^{\frac{1}{3}} \qquad (3-5)$$

Here, the mass transfer coefficient k_c [m/s] is solved by the Sherwood number correlation, d_d [m] is the droplet diameter, $D_{i,m}$ [$m^2 \cdot s^{-1}$] is the diffusivity coefficient and Re_d is the droplet Reynolds number [-], and Sc is the Schmidt number [-]. The right-hand side of equation (3-5) describes the famous Ranz-Marshal correlation [62]. The model constant 0.6 can be replaced by 0.552 in the earlier developed Frossling correlation [63].

$$Nu' = \frac{h d_d}{k} = \frac{\ln(1+B_T)}{B_T}\left(2 + 0.6 Re_d^{\frac{1}{2}} Pr^{\frac{1}{3}}\right) \qquad (3-6)$$

h is the convective heat transfer coefficient [$\frac{W}{m^2 * K}$] calculated by a modified Nu' number, Here k is the thermal conductivity of the gaseous phase (continuous phase) [$\frac{W}{m * K}$]. Pr is the Prandtl number of the continuous phase. d_d is the droplet diameter, and B_T is the Spalding heat transfer number.

Equation (3-7) calculates the enhanced diffusive mass flux due to forced convection in spray simulation:

$$\dot{m}_{diff} = k_c A_d \rho_g (Y_{Fs} - Y_{F\infty}) \qquad (3-7)$$

Where A_d [m^2] is the droplet surface area. The diffusive mass flow rate [kg/s] at the droplet surface can be calculated as:

$$\dot{m}_{diff} = (1 - Y_{Fs})\dot{m} \qquad (3-8)$$

By combining the equation (2-8) with equation (2-7), we have equation (2-9):

$$\dot{m} = \frac{dm}{dt} = k_c A_d \rho_g B_m \qquad (3-9)$$

By combining the altered Sherwood number Sh_{AB} with equation (3-9), the evaporation rate of the single component droplet becomes:

$$Sh' = Sh_{AB} = Sh_0 = Sh * \frac{B_m}{\ln(1 + B_m)} \qquad (3-10)$$

$$\dot{m} = \frac{dm}{dt} = \pi d_d \rho_g D_{i,m} Sh B_m = \pi d_d \rho_g D_{i,m} Sh_{AB} \ln(1 + B_m) \qquad (3-11)$$

Here, the altered Sherwood number Sh' [-] considers the convection term when the relative velocity between the droplet and the continuous gaseous phase is not zero.

Finally, Combining equation (3-11) with equation (3-5), the droplet evaporation rate becomes:

$$\dot{m} = \frac{dm}{dt} = k_c A_d \rho_g \ln(1 + B_m) \qquad (3-12)$$

Where ρ_g [kg $\cdot m^{-3}$] is the gas density, and k_c [m/s] is solved by the Sherwood number correlation.

Heat transfer in single component droplet modelling

The zero-dimensional droplet heating model assumes a uniform droplet temperature inside the evaporating droplet. The model is famous for its simplicity, and the model can largely reduce the computational cost. The Biot number ($Bi = \frac{h}{k} d_d$) can be used to justify the validity of using the 0-D model. When the Biot number is much smaller than unity, the internal heat transfer can be instantaneous compared to the heat transfer between the object surface and ambient environment.

Equation (3-13) describes the 0-D heat transfer model:

$$m_d c_d \frac{dT_d}{dt} = hA_d(T_\infty - T_d) + \frac{dm}{dt}\left(h_{vap}\right) \qquad (3-13)$$

Here, m_d $[kg]$ is the mass of the droplet, and the T_d $[K]$ is the droplet temperature. c_d $[\frac{J}{kg*K}]$ is the droplet heat capacity and the $h_{vap}[J/kg]$ is the droplet/liquid latent heat. T_∞ $[K]$ is the ambient temperature. $hA_d(T_\infty - T_d)$ describes the heat gain/loss from the droplet convection, and the term $\frac{dm}{dt}\left(h_{vap}\right)$ describes the heat loss from liquid evaporation.

3.2 Physical properties

Table 3.1 summarises the physical properties of the air and fuel vapour mixture.

Fuel vapour binary diffusion coefficient in air	Unity Lewis number.
Air/Fuel vapour mixture dynamic viscosity	Constant
Latent heat of evaporation	Yaws. [79] $$L = A\left(1 - \frac{T_d}{T_c}\right)^n$$ $A\ and\ n\ are\ constant$
Liquid specific heat capacity	Sazhin et al. $$C_d = A - B * T_d + C * T_d^{\,2} - C * T_d^{\,3}$$
Liquid density	Yaws [79] $\rho = A * B^{-(1-\frac{T_d}{C})^n}$ $A, B, C\ and\ n\ are\ constant$
Liquid thermal conductivity	Ignored under 0D droplet simulation

Table 3.1. Summary of physical property models used in a single component droplet evaporation simulation

3.3 Multicomponent droplet evaporation

The single-component fuels cannot provide the complex behaviour of the vaporisation in the actual engine spray combustion. Fossil fuels mix with organic oil such as ethanol and methanol, and the evaporation behaves differently from the original components. As more components are introduced in the evaporating fuel, different fuel species leave the droplet from the surface alters the composition of the liquid throughout the droplet lifetime. The mass flux fraction is introduced to determine the fuel composition during evaporation.

$$\varepsilon_i = \frac{Y_{i,v}}{\sum_i Y_{i,v}} \qquad (3-14)$$

The new Spalding mass number is calculated as:

$$B_{m.i} = \frac{(\sum_i Y_{i,v} - \sum_i Y_{i,g})}{(\varepsilon_i - Y_{i,v})} \qquad (3-15)$$

And the evaporation rate of each species is given by:

$$\dot{m}_i = \frac{dm_i}{dt} = k_{c,i} A_d \rho_g \ln(1 + B_{m,i}) \qquad (3-16)$$

Each vapour species has a different binary diffusion coefficient through the air, and the overall evaporation rate can be expressed by equation (3-16) to assume an averaged overall diffusion coefficient. To reduce the complexity of the simulation parameters, the binary diffusion coefficient is calculated based on unity Lewis number and based on the further assumption given by the reference $c_{p,v} = c_{p,g}$, the binary diffusivity is only thermal conductivity dependent. Based on the equation: $Le = \frac{\rho_g D_{i,m} C_{p,v}}{k_g}$ $[-]$. Here, $C_{p,v}$ is the Fuel vapour specific heat capacity, which is assumed to be equal to the gaseous phase's heat capacity. Also, the thermal conductivity of the gaseous phase is assumed to be constant. Therefore, the binary diffusivity (mass diffusivity) coefficient is equal for all fuel components. Table 3.2 defines the physical property for calculating the droplet heat and mass transfer.

Physical property	The rule for multicomponent estimation
Fuel vapour specific heat capacity	$c_{p,v} = \sum_i Y_i C_{p,vi}$
The binary diffusion coefficient in air	Unity Lewis number

Latent heat of evaporation	Presented by Yaws [79] $L = A\left(1 - \frac{T_d}{T_c}\right)^n$ $A\ and\ n\ are\ constant$
Liquid thermal conductivity	Ignored by assuming unity temperature and mass fraction (0-D) law

Table 3.2. Physical property used in multicomponent droplet simulations.

The heat transfer equation can be modified as:

$$m_d c_d \frac{dT_d}{dt} = hA_d(T_\infty - T_d) + \sum_i \frac{dm_i}{dt}\left(h_{vap,i}\right) \qquad (3-17)$$

Here, m_d $[kg]$ is the mass of the droplet, and the T_d $[K]$ is the droplet temperature. c_d $[\frac{J}{kg*K}]$ is the droplet heat capacity and the $h_{vap,i}[J/kg]$ is the latent heat of each component. $\sum_i \frac{dm_i}{dt}(h_{vap,i})$ is the evaporation rate for all components $[kg/s]$. T_∞ is the ambient temperature $[K]$.

3.3.1 Vapour-liquid equilibrium for multicomponent evaporation

Droplet vapourisation is a two-phase problem; the vapour-liquid equilibrium (VLE) is crucial for determining species transfer rate in two phases. The liquid mixture may be ideal or non-ideal depending on the liquid species' molecules, and the gas phase can be non-ideal under higher pressure. At equilibrium, liquid mole concentration of component i is related to the vapour mole concentration x_i^v [-] of component i.

$$f_i^v = x_i^v \varphi_i^v p = x_i^L \varphi_i^L p = f_i^L \qquad (3-18)$$

Where x_i^v [-] and x_i^L [-] are the vapour and liquid mole fractions, respectively. φ_i^v [-] and φ_i^L [-] are the fugacity coefficients. The p is ambient pressure.

The fugacity of pure liquid i at ambient temperature T and ambient pressure p is calculated as:

$$f_i^L(T,p) = \gamma_i x_i^L \varphi_{sat,i}^L P_{sat,i} exp\left(\frac{V_i^L\left(p - P_{sat,i}\right)}{RT}\right) \qquad (3-19)$$

Where $P_{sat,i}$ is the saturated vapour pressure and the molar liquid volume V_i^L is calculated by the ratio of the molecular weight to the component density. γ_i is the activity coefficient, and the exponential term is the Poynting factor and is assumed to be negligible. The $\varphi_{sat,i}^L$ and φ_i^v are assumed to be unity under low-pressure conditions. Further, equation 2-30 becomes Raoult's law if the liquid phase is also considered ideal.

$$x_i^v p = x_i^L P_{sat,i} \qquad (3-20)$$

Raoult's law is a simplified method for calculating Vapour-liquid equilibrium and is widely used in research studies. The law assumes that each component's partial vapour pressure is self-independent and can only calculate reasonable solution behaviour when the molecular species are not too different in size and have the same chemical nature. The constituents of a solution are normally intimately intermixed, and the partial properties cannot vary independently as molecular interactions affect each component's properties in the mixture [63]. When actual vapour concentrations can not demonstrate linear relations for a solution's behaviour, the activity coefficients express Raoult's law deviations.

The activity coefficients alter when different functional groups are in the liquid mixture as the net intermolecular forces arise. When alcohol is

mixed with gasoline or diesel, the non-ideality phenomenon becomes significant due to the -OH (alcohol) functional group [3, 4, 19, 27]. The activity coefficients may be much larger than unity based on the experimental study from wen et al. [19]. Therefore, the activity coefficient should be included in the VLE model.

$$x_i^v p = \gamma_i x_i^L P_{sat,i} \qquad (3-21)$$

Various numerical methods for defining the activity coefficient γ_i are widely used and presented in [1, 25]. i.e. Van Laar, Wilson, NRTL, UNIQUAC, and UNIFAC. NRTL and UNIFAC models are the most accurate models for calculating the γ_i.

The NRTL model is fitted to experimental binary VLE data, and it is the most accurate numerical method. However, the model strongly requires different sets of experimental data, and the fitting process may become tedious with the increase in the number of liquid species.

The activity coefficients are modelled using the UNIFAC method for mixtures with no vapour-liquid equilibrium data or many components. This method requires only pure single-component data tested experimentally. It can provide a reasonable estimate for a mixture containing azeotropes. The boiling point for both components is the same due to molecular differences. The calculation for the UNIFAC method can be separated into two parts. The first part is the combinatorial part [6], which describes the molecular interactions due to molecule shape and size differences. The second part of the model is the residual part, which describes functional group interactions.

The activity coefficient in the UNIFAC model can be calculated as:

$$ln\gamma_i = ln\gamma_i^C + ln\gamma_i^R \qquad (3-22)$$

The combinatorial part $ln\gamma_i^C = f(X_i, r_i, q_i)$, Accounts for the molecular size and the Residual part $ln\gamma_i^R = f(X_i, r_i, q_i, T_d, a_{mn})$ Accounts for energetic interactions between Molecules.

In equation (3-22), the combinatory part can be calculated as:

$$ln\gamma_i^C = ln\frac{\Phi_i}{X_i} + 5 \times q_i ln\frac{\theta_i}{\Phi_i} + l_i - \frac{\Phi_i}{X_i}\sum_j X_j l_j \qquad (3-23)$$

$$l_i = 5(r_i - q_i) - (r_i - 1) \qquad (3-24)$$

$$\theta_i = \frac{q_i X_i}{\sum_j X_j q_j} \qquad (3-25)$$

$$\Phi_i = \frac{r_i X_i}{\sum_j X_j r_j} \qquad (3-26)$$

Here, X_i is the mole fraction of component i, θ_i is the area fraction and the Φ_i is the segment fraction (volume fraction). Pure component parameters r_i and q_i are, respectively, measures of molecular van der Waals volumes and molecular surface areas. The q_i and r_i can be calculated by the sum of the group volume and area parameters R_k and Q_k.

$$R_k = \sum_k \frac{V_{wk}}{15.17}, \qquad Q_k = \sum_k \frac{A_{wk}}{2.5 \times 10^9} \qquad (3-27)$$

In equation 3-27, the normalisation factors 15.17 and 2.5×10^9 are determined by the volume and external surface area of a $-CH_2$ unit in polyethene.

And q_i and r_i can be calculated as:

$$q_i = \sum_k v_k^{(i)} Q_k \,, r_i = \sum_k v_k^{(i)} R_k \qquad (3-28)$$

Where $v_k^{(i)}$ is the number of occurrences of the functional group i.

Then the residual part can be calculated as:

$$ln\gamma_i^R = \sum_k v_k^i (ln\Gamma_k - ln\Gamma_k^i) \quad (3-29)$$

$$ln\Gamma_k = Q_k \left[1 - \ln\left(\sum_m \theta_m \Psi_{mk}\right) - \sum_m \frac{\theta_m \Psi_{km}}{\sum_n \theta_n \Psi_{nm}}\right] \quad (3-30)$$

$$\Psi_{mn} = \exp\left(-\frac{\boldsymbol{a}_{mn}}{T_d}\right) \quad (3-31)$$

$$\theta_m = \frac{Q_m X_m}{\sum_n X_n Q_n} \quad (3-32)$$

Where, Ψ_{mn} is the group-interaction parameter calculated by the parameter $\boldsymbol{a}_{mn}\,[K]$, and droplet temperature $T_d\,[K]$ and θ_m is the secondary group area fraction.

Table 3.3 and 3.4 Demonstrates the main and secondary function groups of iso-octane and ethanol mixture.

Name	Main No.	Sec. No.	v[-]	R [-]	Q[-]
$-CH_3$	1	1	5	0.9011	0.848
$-CH_2$	1	2	1	0.6744	0.54
$-CH$	1	3	1	0.4469	0.228
$-C$	1	4	1	0.2195	0

Table 3.3 Functional groups of iso-octane.

Name	Main No.	Sec. No.	v[-]	R [-]	Q[-]
$-CH_3$	1	1	5	0.9011	0.848
$-CH_2$	1	2	1	0.6744	0.54
$-OH$	5	14	1	1	1.2

Table 3.4 Functional groups of ethanol.

Component	Main Group No.	$\boldsymbol{a}_{mn}[K]$
Isooctane	1	$\boldsymbol{a}_{1,5} = 986.5$
Ethanol	1, 5	$\boldsymbol{a}_{1,5} = 986.5$
		$\boldsymbol{a}_{5,1} = 156.4$

Table 3.5 Group interaction parameter of each component

Implementing the UNIFAC method into the simulation demonstrates a dramatic difference between the original Raoult's Law. The nonideality effects described by the activity coefficient is shown in figure 2.1.

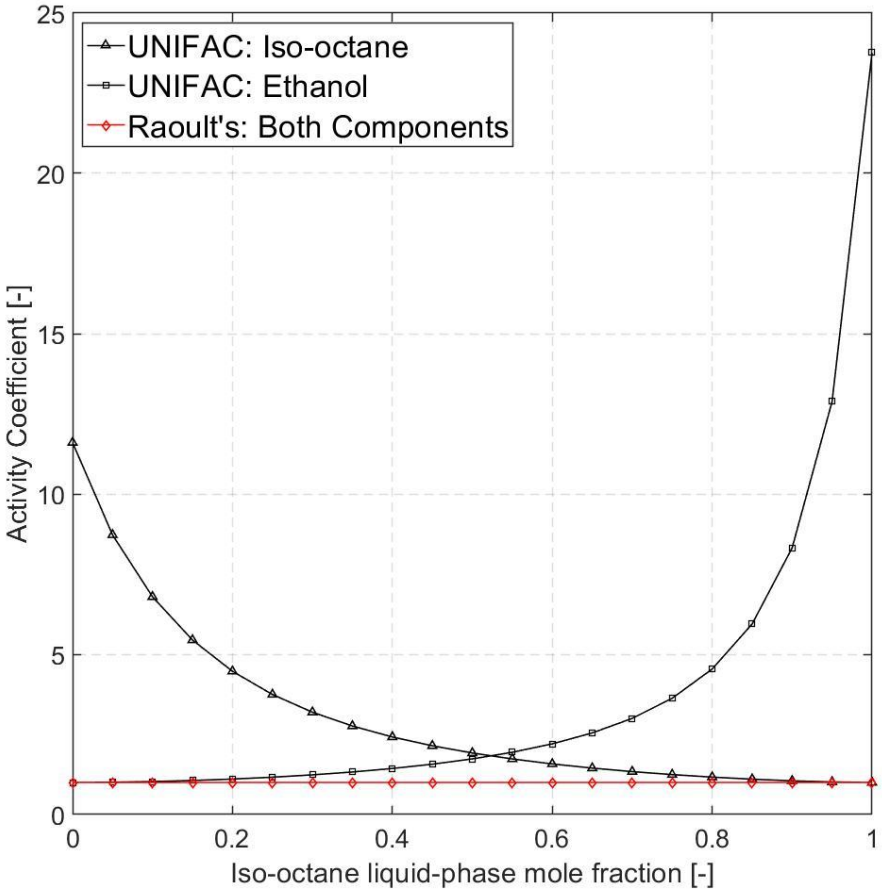

Figure 3.1. The activity coefficients γ of ethanol and iso-octane for a binary-component ethanol/iso-octane mixture at droplet temperature 300K

Figure 3.1 demonstrates ethanol and iso-octane activity coefficients in a binary-component liquid mixture at the liquid phase with a temperature of 300K simulated by both UNIFAC and Raoult's method. The graphic shows the activity-coefficient rise dramatically when one component becomes minor in the liquid mixture. The difference between the two methods might reach 24 times as the component ethanol approaches the maximum. The graphic implies that even a less 'volatile' (low saturated vapour pressure) component in the mixture might be possible to evaporate faster at the droplet surface than a volatile component.

The temperature-composition phase diagram T-XY chart of the binary component ethanol/iso-octane mixture at P=1 bar determined by Raoult's law and the UNIFAC law is illustrated in Figure. 3.2 and compared to published data [19].

The relation of the magnitudes of the liquid- and vapour-phase mole fractions of ethanol is separated by the azeotrope point. On the left side, the mole fraction of ethanol at the liquid phase is bigger than its vapour phase and the opposite at the right side. The Figure shows a good comparison between UNIFAC with experimental data has been achieved, including the minimum-boiling azeotrope. Compared with Raoult's law, the experimental data has shown a different trend.

The ability to simulate evaporation dynamics of a multicomponent liquid-fuel mixture will be minimal by adopting Raoult's law. Therefore. A more realistic evaporation model should be considered since Raoult's law cannot accurately simulate the liquidus and vaporous curves.

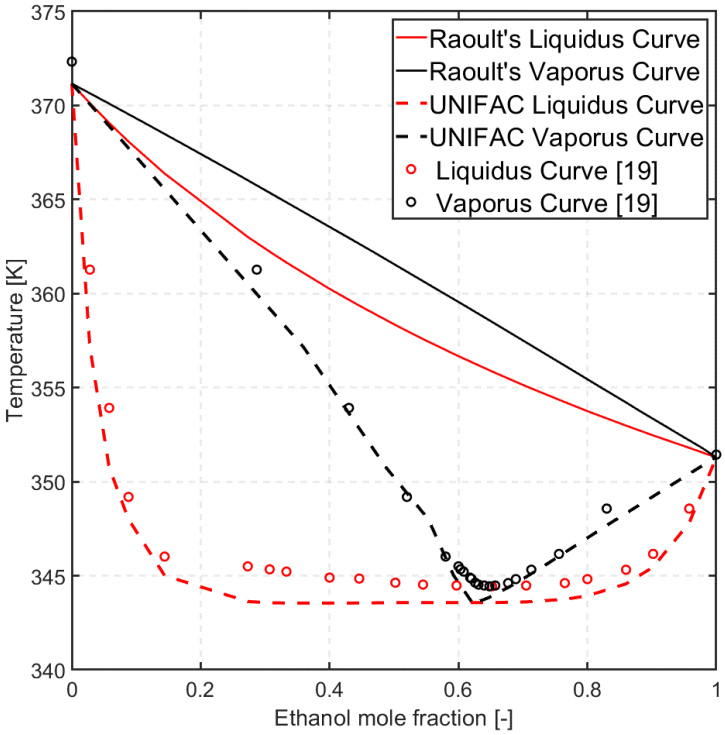

Figure 3.2. Ethanol/iso-octane phase diagram at 1 bar

3.4 Droplet Boiling modelling

The droplet boiling temperature defines the boiling process of a single component droplet. When the droplet temperature reaches the boiling point, the vapourisation (boiling) rate can be computed by solving equation (3-33)

$$\frac{d(d_p)}{dt} = \frac{2k_g}{\rho_d c_{p,g} d_d}\left(2 + 0.6Re^{\frac{1}{2}}Pr^{\frac{1}{3}}\right)\ln\left[1 + \frac{c_{p,g}(T_\infty - T_d)}{h_{fg}}\right] \qquad (3-33)$$

Where k_g is the thermal conductivity of the gas $[W/(m * k)]$.

If the total vapour pressure is higher than the ambient pressure, the Multicomponent Boiling equation will be applied to the simulation.

Two methods for calculating the total vapour pressure depend on the vapour-liquid equilibrium, the ideal Raoult's law, and the non-ideal law. The total vapour pressure based on the ideal law can be calculated as:

$$p_{tot} = x_i p_{sat,i} + x_j p_{sat,j} \qquad (3-34)$$

The total vapour pressure based on the non-ideal law is calculated as:

$$p_{tot} = \gamma_i x_i p_{sat,i} + \gamma_j x_j p_{sat,j} \qquad (3-35)$$

3.5 Numerical scheme for solving ODE

The infinite conductivity and diffusivity (zero-dimensional) droplet model is used in most numerical codes. The vapourisation process of a single droplet has been simplified into an ODE problem. Time scheme like Backward Euler, Runge-Kutta is widely used for solving the RHS of the equation. There are four numerical schemes available in ANSYS FLUENT: Exponential integral, implicit Euler, trapezoidal and 5th order Runge-Kutta scheme. The implicit Euler is the default function, and the 5th order Cash-Karp-Runge-Kutta scheme will provide an embedded error control.

3.6 Physical property averaging

The properties will depend on local vapour composition and temperature. A reference value of both species and temperature at the gas phase is required to decide the liquid phase's physical properties.

$$T_{ref} = T_d + \alpha_T (T_g - T_d) \qquad (3-36)$$

Here, T_{ref} [K] is the reference temperature, and T_d [K] is the droplet temperature based on the lumped model and T_g is the temperature at the gas phase. α_T [-] is the averaging coefficient for temperature defined as 1/3.

$$Y_{ref} = Y_{d,i} + \alpha_Y\left(Y_{g,i} - Y_{d,i}\right) \qquad (3-37)$$

Here, Y_{ref} [-] is the reference mass fraction, $Y_{g,i}$ [-] and $Y_{d,i}$ [-] are the evaporation species mass fraction in the far-field gas mixture and at the droplet surface, respectively. α_Y [-] is the averaging coefficient for mass fraction and $\alpha_Y = \frac{1}{3}$ [26].

Finally, the solution procedure in each time step of a droplet can be calculated as follows:

1. Obtain thermodynamic properties and the species composition of the ambient gas, including ρ_g, T_g, $Y_{i,g}$;
2. Determine transport and thermodynamic properties of the two phases, including c_d $[\frac{J}{kg*K}]$, $c_{p,g}$, $D_{i,m}$ and $h_{vap,i}$[J/kg].
3. Determine dimensionless numbers Re_d, Pr, Sc.
4. Obtain species compositions $Y_{i,V}$ at the droplet surface using evaporation models.
5. Determine the heat and mass transfer Spalding numbers B_T and $B_{m,i}$.
6. Determine the heat and mass transfer coefficients.
7. Determine the evaporation rate of each component.
8. Determine the droplet temperature T_d.
9. Determine the droplet size.

3.7 Numerical Model for spray simulation

The Discrete Phase Model (DPM) is used to study the spray vapourisation process in this work. In DPM, the discrete liquid droplets, also known as “parent droplets”, replace the liquid column's continuous phenomena from the nozzle exit. The droplets normally have the same diameter as the nozzle. An algorithm (Breakup model) for dividing each parent droplet into a smaller child droplet resembles the spray formation. The parameters in the algorithm require tuning so that the CFD simulation results can match the experimental data. Therefore, the algorithm is only applicable to certain spray simulations that can be easily tuned to match the results [34,35]. The tuning process is demonstrated in figure 1.9. A detailed, well-examined experimental data is essential for the spray simulation using the Lagrangian model as the breakup process is a tunning factor.

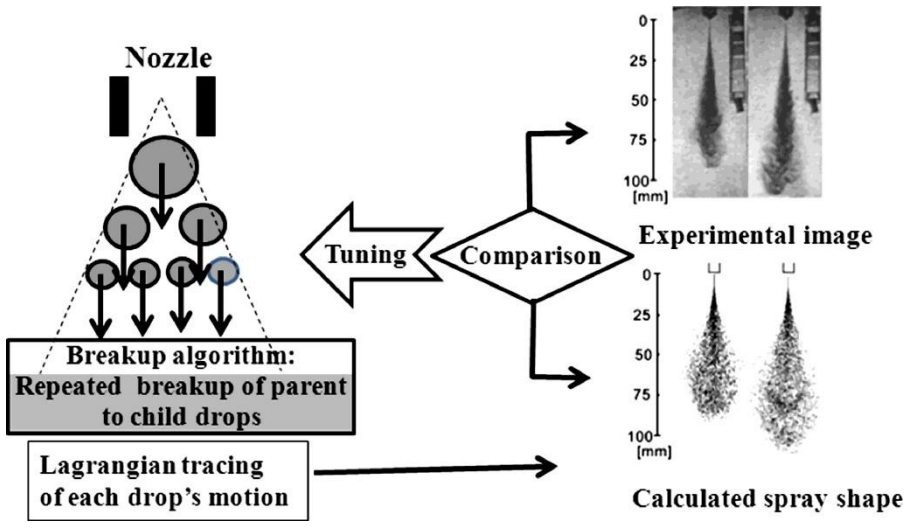

Figure 3.3. The Lagrangian model applied in spray simulation

3.7.1. Models in DPM for spray vapourisation simulation

The single droplet evaporation model is used as a sub-model for simplifying the two-phase flow simulation. The numerical approach uses Lagrangian Particle tracking to model the dispersed liquid phase. The liquid phase is simplified as moving particles/droplets, and each particle is tracked until its fully evaporated and converted to the vapour phase. The particles are introduced by a parcel injection method, and each parcel contains many droplets that coexist at the same location with the same properties. i.e. diameter, velocity, temperature, mass. The parcel injection method reduces the computational cost compared with individual particle tracking. The method is widely adopted in many CFD codes such as FLUENT, OpenFOAM, Star-CD, Converge, etc. The N-S equation solves the gaseous/vapour phase. The additional source terms include mass, heat, momentum, and species, will be updated from the Lagrangian phase to the continuity equation. The sources terms account for the mass added to the gas phase by evaporation and the energy and momentum exchange that the droplets will have with the gas phase. Other submodels, including atomisation, breakup, droplet collision, and spray-wall interaction my also be introduced in the simulation.

3.7.1.1 Primary breakup models

One of the breakup mechanisms is caused by nozzle cavitation. In a spray injector, the sharp nozzle entrance increases the turbulent level and causes cavitation. The cavitation generates the in nozzle vapour bubbles, and the bubbles may implode inside the liquid enhance the breakup

mechanism at the nozzle exit. Reynolds number, Ohnesorge number, and Weber number are introduced to identify the breakup phenomenon:

$$We = \frac{Drag\ Force}{Cohesion\ Force} = \frac{\rho_l v l}{\sigma} \qquad (3-38)$$

$$Oh = \frac{\mu_l}{\sqrt{\rho_d \sigma l}} \qquad (3-39)$$

Here, ρ_l $[kg/m^3]$ is the droplet/liquid density, l is the characteristic length scale that equal to the droplet diameter d_d $[m]$, σ $[N/s]$ is the surface tension of the liquid and the μ_l is the dynamic viscosity of the liquid. v is the liquid velocity.

The breakup regimes can be classified into three different regimes based on Ohnesorge number, Weber number, and gas-liquid density ratio $\frac{\rho_g}{\rho_l}$ [-] :

1. Rayleigh regime, the liquid core will break up into identical droplet sizes at low Reynolds number, and the process is controlled by surface tension and liquid oscillating force.
2. Wind-induced regime. The wind-induced regime happens at intermediate Reynolds number, and the aerodynamic force will affect the droplet formation during the breakup.
3. Atomization regime. The atomization regime forms at a high Reynolds number, and the liquid jet disintegrates immediately at the nozzle exit.

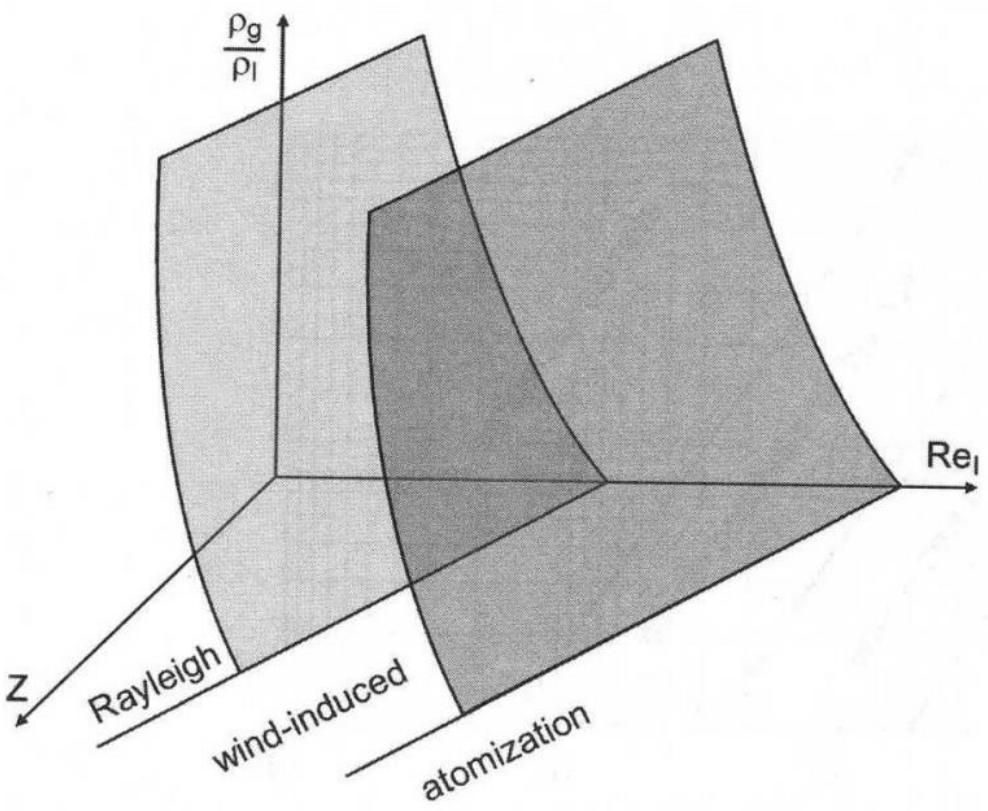

Figure 3.4. Liquid jet breakup regimes defined by Reitz [80]

The cavitation is one of the key features in a nozzle design, and the phenomenon has a significant impact on spray simulation. In general, the primary breakup can be accurately captured by using the Eulerian and VOF approach. These approaches also provide a reasonable result of cavitation. However, the nozzle diameter of an injector is normally around one millimetre, and both models require an accurate nozzle geometry that massively increases the computational cost.

In the Discrete phase method, there are two different approaches to capture the primary breakup phenomenon:

1. An atomizer numerical model accounts for nozzle effects such as cavitation and turbulence. The model identifies the initial droplet size at the nozzle exit.

2. The nozzle discharge coefficient can be considered with the experimental data. However, most of the injector does not have sufficient data to provide an accurate coefficient. A Blob method ignores the nozzle effect, and the primary breakup process has been simplified into a cluster of uniform droplets.

RD Reitz et al. defined the diesel internal nozzle motion into five categories. Namely, turbulent flow, cavitation, supercavitation, hydraulic flip, and partly reattached flow [17]. Most of the fluid flow does not attach to the internal boundary of the nozzle (wall). Therefore, a discharge coefficient may be applied to model the initial droplet velocity at the nozzle exit. The mean mass flow rate is always lower than the estimation from Bernoulli's equation.

The numerical code FLUENT provides a Plain-Orifice atomizer model to consider the in-nozzle effect on the initial droplet velocity and size distribution. The model simplified the five different categories into three different regimes. Figure 1.11. demonstrates the calculated regimes by the existing Plain-Orifice atomizer model.

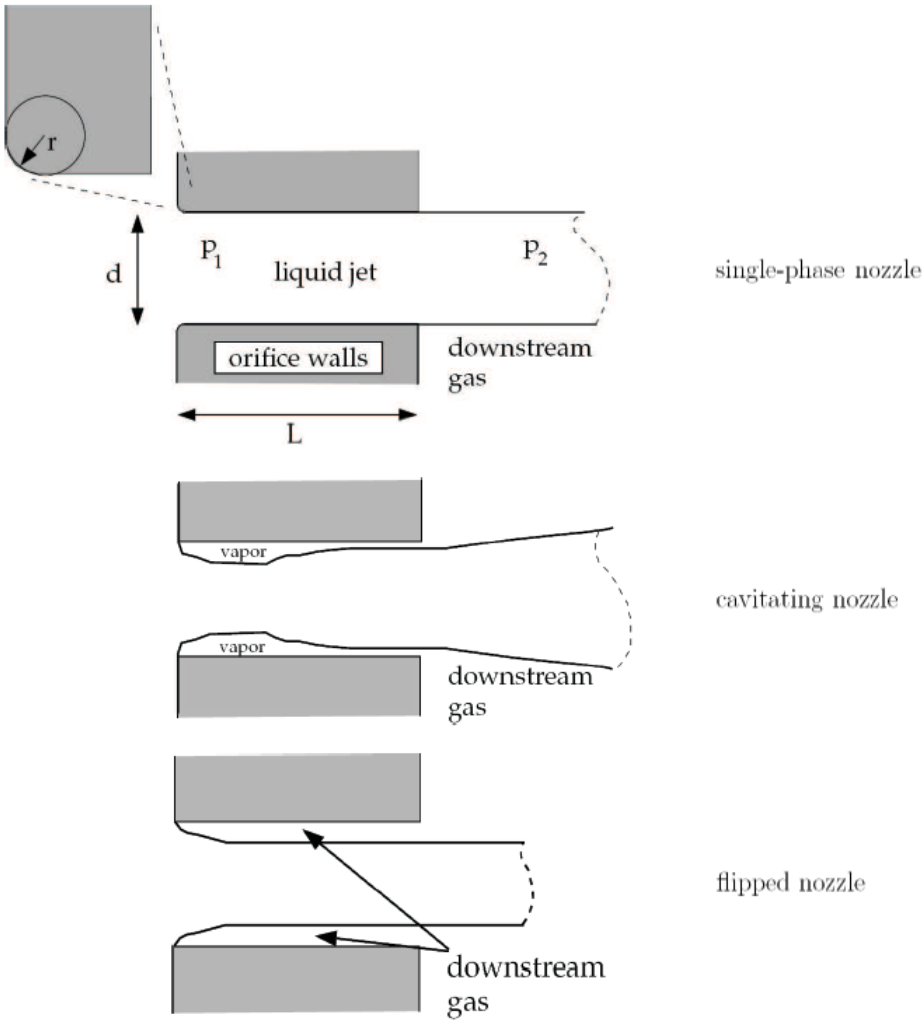

Figure 3.5. Possible nozzle flows defined by Plain-Orifice Atomizer [26].

However, the initial parameters for the atomizer model are complex and difficult to gather. The parameters include nozzle diameter, length, inlet corner radius, injection pressure, in-chamber ambient pressure, liquid density, vapour pressure, and viscosity are required to generate the initial droplet size and velocity. Therefore, a spray simulation for IC engines may ignore the effect of nozzle cavitation and directly use Bernoulli's equation to define the initial spray condition.

The "Blob" method introduced by Reitz et al.simplifies the primary breakup phenomena. A cluster of droplets represents the liquid core at the nozzle

exit with the same size as the actual injector nozzle. Then, the droplets are tracked by using the Lagrangian parcel tracking method. Further, the initial droplet size can be modified to match the experimental data [35].

The initial conditions such as droplet velocity [m/s], temperature [K], size/diameter [r_d], and mass flow rate [kg/s] are the fundamentals that contribute to an accurate spray simulation.

3.7.1.2 Secondary breakup models

After the liquid ligament is detached from the continuous liquid core during the primary breakup, the liquid ligament will disintegrate into smaller droplets. In CFD simulation, this phenomenon can be simulated based on the Ohnesorge number (Oh) and Weber number (We). The Ohnesorge number and the Weber number calculation is shown in equation 1.1 and 1.2.

Ohnesorge number is dimensionless based on the liquid phase's viscous forces to inertial and surface tension forces. The Weber number is dimensionless and used for analyzing the fluid flow with an interface to determine the breakup type.

According to the Weber number, three different secondary breakup mechanisms are proposed by Liu [37]. The three breakup mechanisms are shown as follow:

1. Bag breakup ($6 \leq We < 80$)
2. Stripping breakup ($80 \leq We < 350$)
3. Catastrophic breakup ($We > 350$)

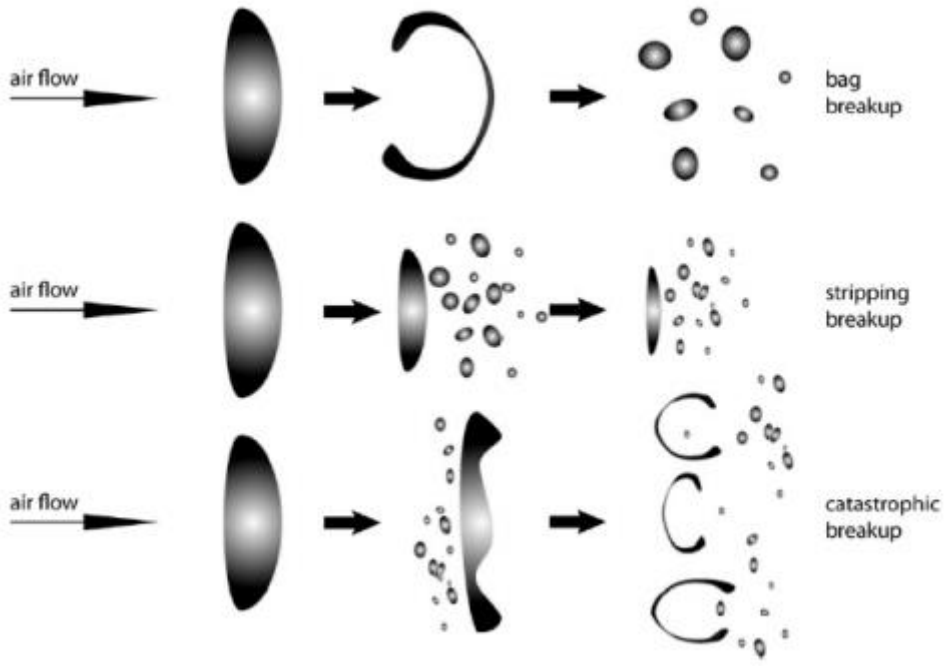

Figure 3.6. Different types of secondary breakup [66]

Both Ohnesorge number (Oh) and Weber number (We) are used to calculate the breakup time in different secondary breakup sub-models. Such as TAB, Wave, and KH-RT models.

3.7.1.2.1 Wave Breakup Model

The Wave breakup model is appropriate for high-weber-number flows developed by Reitz [26]. The model assumes the time of breakup and the resulting droplet size are based on the fastest-growing Kelvin-Helmholtz instability derived from the jet stability analysis.

In the wave model, the radius of a newly formed droplet can be calculated as:

$$r = B_0\Lambda \qquad (3-40)$$

Here, B_0 is a constant model set equal to 0.61, Λ is calculated in equation (2-49)

$$\frac{\Lambda}{a} = 9.02\frac{(1+0.45Oh^{0.5})(1+0.4Ta^{0.7})}{\left(1+0.87We_g^{1.67}\right)^{0.6}} \qquad (3-41)$$

Here, Oh is the Ohnesorge number [-] calculated as $Oh = \frac{\sqrt{We_d}}{Re_d}$, $We_d = \rho_d U^2 a/\sigma$ and $We_g = \rho_g U^2 a/\sigma$ are the liquid and gaseous Weber number [-]. ρ_L is the liquid (droplet) density [kg/m^3]. a is the nozzle diameter [m] and the initial parcel diameter. and Ta is the Taylor number [-] calculated as $Ta = Oh\sqrt{We_2}$.

The rate of change of droplet radius in the parent parcel is given by:

$$\frac{da}{dt} = -\frac{(a-r)}{\tau}, r \leq a \qquad (3-42)$$

Here the breakup time τ [s] can be calculated as:

$$\tau = \frac{3.726\mathrm{B_1a}}{\Lambda\Omega} \qquad (3-43)$$

Here, the coefficient B_1 [-] is a tuning factor that varies from 1 to 60. the maximum growth rate Ω in equation (3-43) can be calculated as:

$$\Omega\sqrt{\frac{\rho a^3}{\sigma}} = \frac{0.34+0.38We_g^{1.5}}{(1+Oh)(1+1.4Ta^{0.6})} \qquad (3-44)$$

3.7.1.2.2 KH-RT Breakup Model

The KH-RT model combines Kelvin-Helmholtz waves driven by the aerodynamic forces with Rayleigh-Taylor instabilities based on the acceleration of the shed drops ejected into freestream conditions. The model cannot be applied to the sprays with a low-Weber number.

Here, the Rayleigh-Taylor Breakup model can be calculated as:

$$\Omega_{RT} = \sqrt{\frac{2\left(-g_t(\rho_d - \rho_g)\right)^{\frac{3}{2}}}{3\sqrt{3\sigma}(\rho_d - \rho_g)}} \qquad (3-45)$$

Equation 3-45 calculates the frequency of the fastest-growing wave. Where g_t is the acceleration of the droplet. The wavenumber can be calculated as:

$$K_{RT} = \sqrt{\frac{-g_t(\rho_d - \rho_g)}{3\sigma}} \qquad (3-46)$$

The breakup time for the RT model can be calculated as:

$$\tau_{RT} = \frac{C_\tau}{\Omega_{RT}} \qquad (3-47)$$

Here C_τ is the RT breakup time constant with a default value 0.5 [-]

The child droplet can be calculated as:

$$r_c = \frac{\pi C_{RT}}{K_{RT}} \qquad (3-48)$$

C_{RT} is the breakup radius constant with a default value of 0.1.

3.7.1.3 Droplet Drag models

The ambient gaseous phase decelerated the liquid/droplet during the spray vapourisation process. Equation 3-49 describes the spherical drag law, and 1.4 is used to calculate dynamic drag law.

$$C_D = a_1 + \frac{a_2}{Re} + \frac{a_3}{Re^2} \qquad (3-49)$$

Where a_1, a_2, and a_3 are model constants, and Re is the droplet Reynolds number.

$$C_D = \begin{cases} 0.424\ (Re > 1000) \\ \frac{24}{Re}\left(1 + \frac{1}{6}Re^{\frac{2}{3}}\right)\ (Re \leq 1000) \end{cases} \quad (3-50)$$

The Eulerian-Lagrangian approach, also known as the Discrete Phase Model. The gaseous phase is recognised as a continuum solved by N-S equations. In contrast, the discrete phase (Liquid phase for spray simulation) is calculated by tracking many particles or droplets throughout the numerical domain. Further, the discrete phase updates or exchanges the momentum, mass, and energy with the continuous phase.

The E-L approach is adopted as the numerical model is widely used in academia and industry. The approach requires the dispersed phase with a low volume fraction in the domain for coupling with the simulation's continuous gas phase.

3.7.1.3 Equations for Particles motion

For a Lagrangian particle droplet, the correlation between the force acting on a discrete phase particle and the particle inertia can be written as:

$$m_p \frac{d\overrightarrow{u_p}}{dt} = m_p \frac{\vec{u} - \overrightarrow{u_d}}{\tau_r} + m_p \frac{\vec{g}(\rho_d - \rho)}{\rho_p} + \vec{F} \quad (3-51)$$

Here, m_d is the droplet mass [kg], $\overrightarrow{u_p}$ is the droplet velocity [m/s], $\vec{u}$ and ρ_g are the velocity and density of the gaseous phase, respectively, $\vec{F}$ is

additional force [N], $m_p \frac{\vec{u}-\overrightarrow{u_d}}{\tau_r}$ is the drag force [N] and τ_r is the droplet relaxation time calculated as: $\tau_r = \frac{\rho_d d_d^2}{18\mu} \frac{24}{C_{drag} Re}$. Where μ is the molecular viscosity of the gaseous phase, d_d is the droplet diameter, C_{drag} is the drag coefficient applies on the droplet using the spherical Drag law given by Morsi et al. [5], and Re is the relative Reynolds number defined as:$Re \equiv \frac{\rho_g d_d |\overrightarrow{u_d}-\vec{u}|}{\mu}$.

3.7.1.4 Coupling between Gaseous phase and dispersed phase

There are two coupling functions for an E-L approach simulation. An uncoupled approach (one-way coupling) only includes the effect from the continuum (gaseous phase). In contrast, the coupled approach (two-way coupling) updates the discrete phase's impact on the continuum. For modelling spray evaporation, the coupled approach should be selected.

3.7.1.4.1 Governing equation for the continuous phase

The spray evaporation process requires four equations for modelling the momentum, mass, heat, and species transfer. The equations are concluded as follow:

$$\frac{\partial \rho}{\partial t} + \nabla \cdot (\rho \vec{v}) = S_m \qquad (3-52)$$

Equation 3-52 describes the mass conservation for the continuous phase and the S_m $[kg]$ is the additional mass source due to droplet vapourisation.

$$\frac{\partial(\rho\vec{v})}{\partial t} + \nabla \cdot (\rho\vec{v}\vec{v}) = -\nabla \mathrm{p} + \nabla \cdot (\bar{\bar{\tau}}) + \rho\vec{g} + \vec{F} \qquad (3-53)$$

Equation 3-53 describes momentum conservation. Where $\vec{F}$ is the additional force issued by external body force and $\rho\vec{g}$ is gravitational body force. The stress tensor $\bar{\bar{\tau}}$ is calculated as:

$$\bar{\bar{\tau}} = \mu\left[(\nabla\vec{v} + \nabla\vec{v}^{T}) - \frac{2}{3}\nabla\vec{v}I\right] \qquad (3-54)$$

$$\frac{\partial(\rho E)}{\partial t} + \nabla \cdot \left(\vec{v}(\rho E + p)\right) = \nabla \cdot \left(k_{eff}\nabla \mathrm{T} - \sum_{j} h_j\vec{J}_j + \left(\bar{\bar{\tau}}_{eff} \cdot \vec{v}\right)\right) + S_h (3-55)$$

$$E = h - \frac{p}{\rho} + \frac{v^2}{2} \qquad (3-56)$$

$$h = \sum_{j} Y_j h_j + \frac{p}{\rho}, h_j = \int_{T_{ref}}^{T} c_{pg,j}dT \qquad (3-57)$$

Where T_{ref} is 298.15 $[K]$. h is the sensible enthalpy.

Equation 3-55 describes the energy conservation for the continuous phase. Where S_h is the additional heat source.

$$\frac{\partial(\rho Y_i)}{\partial t} + \nabla \cdot (\rho\vec{v}Y_i) = -\nabla \cdot \vec{J}_i + R_i + S_i \qquad (3-58)$$

Where R_i is species production net rate due to chemical reaction, and S_i is production rate from an additional source. i.e. Discrete phase droplet evaporation.

3.7.1.4.2 Parcel Injection method

The particle injection's mass flow rate is a key parameter that determines the absolute value of the DPM sources. The mass flow rate $\dot{m}_s$ $[kg/s]$ can

be converted into the number of particles injected per time step. However, tracking individual particles is computational cost consuming, and it is not feasible in practical spray simulation. Therefore the 'parcel' method represents a cluster of droplets with the same parameter to reduce the computational cost. The number of particles in each parcel can be calculated using a parcel release method. The default calculation method can is shown in Equations 3-59.

$$NP = \dot{m}_s \frac{\Delta t}{m_d} \qquad (3-59)$$

Where NP [-] is the number of the particle, $\dot{m}_s$ Is the mass flow rate of the particle stream, Δt is the time step in a transient simulation. m_d is the particle mass calculated based on the initial droplet diameter.

The cone injection and the plain-orifice atomizer are widely used in Engine spray simulation to resemble the liquid shape. The cone injection method is the simplest function to model Engine spray in DPM. It requires an additional cone angle ϑ to model the near nozzle exit spray. The cone angle is normally calculated based on the spray angle issued by the experimental data or using the equation developed by many researchers. Reitz develops the numerical equation for defining the spray angle.

$$\tan\left(\frac{\vartheta}{2}\right) = \frac{2\pi}{3C_a}\sqrt{\frac{3\rho_A}{\rho_f}} \qquad (3-60)$$

Another injection function is the plain-orifice atomizer introduced in chapter 1. Based on the nozzle geometry parameters, the model calculates the initial 'Blob' diameter and velocity. The flowchart for defining the initial conditions is shown in figure 2.5.

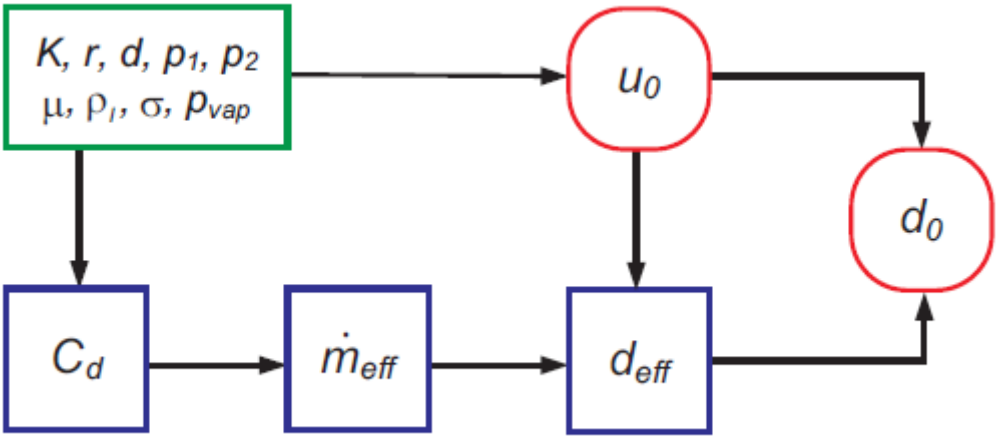

Figure 3.7. schematic flow chart of the plain-orifice atomizer.

3.7.1.4.3 Momentum transfer between the Discrete phase and Continuous phase

The momentum transfer from the continuous phase to the discrete phase is computed as:

$$F = \sum \left(\frac{18 \mu_g C_D Re}{\rho_d d_d^2 24} (u_d - u_g) + F_{other} \right) \dot{m}_d \Delta t \qquad (3-61)$$

Here, μ is the viscosity of the gaseous phase $[Pa \cdot s]$, u_d is the droplet velocity [m/s], u is the velocity of the gaseous phase $[m/s]$. And $\dot{m}_d$ is the mass flow rate of the particles. Δt is the time step $[s]$ and F_{other} is the other interaction forces $[N]$.

3.7.1.4.4 Heat transfer between the Discrete phase and Continuous phase

$$Q = \frac{\dot{m_{d,0}}}{m_{d,0}}\left[\left(m_{d_{in}} - m_{d_{out}}\right)\left[-H_{lat_{ref}}\right] - m_{d_{out}}\int_{T_{ref}}^{T_{d_{out}}} C_d dT + m_{d_{in}}\int_{T_{ref}}^{T_{d_{in}}} c_d dT\right] \quad (3-62)$$

Here, $\dot{m_{d,0}}$ is the initial mass flow rate of the particle injection [kg/s], and $m_{d,0}$ [kg] is the initial mass of the particle, $m_{d_{in}}$ is the mass of the particle on cell entry [kg], $m_{d_{out}}$ [kg] is the mass of the particle on the cell exit. C_d $[\frac{J}{kg*K}]$ is the heat capacity of the particle, $T_{d_{in}}$ [K] is the temperature of the particle on cell entry and the $T_{d_{out}}$ [K] is the temperature of the particle on the cell exit. T_{ref} is the reference temperature for enthalpy (K) and $H_{lat_{ref}}$ [J/kg] is the latent heat at reference conditions that is calculated as:

$$H_{lat_{ref}} = H_{lat} - \int_{T_{ref}}^{T_{bb}} C_{p,g} dT + \int_{T_{ref}}^{T_{bb}} C_d dT \quad (3-63)$$

3.7.1.4.5 The mass exchange between two phases

The mass transfer from the discrete phase to the continuous phase in an evaporation simulation is calculated by changing the particle's mass as it passes through each cell in the numerical domain.

$$M = \frac{\Delta m_d}{m_{d,0}} \dot{m}_{d,0} \quad (3-64)$$

Here, Δm_d [kg] is the change of the mass due to evaporation in one cell. $m_{d,0}$ is the mass source or the injection mass flow rate of the system.

3.7.1.4.6 Under-Relaxation of the Phase exchange

The phase exchange of heat, mass, and momentum between the continuous and discrete phases is calculated through an under-relaxed factor.

The additional force $\vec{F}$, heat Q, and mass M, can be calculated as:

$$M_{n+1} = M_n + \alpha_R(M - M_n) \quad (3-65)$$

$$F_{n+1} = F_n + \alpha_R(F - F_n) \quad (3-66)$$

$$Q_{n+1} = Q_n + \alpha_R(Q - Q_n) \quad (3-67)$$

Here, M, Q, F are from equations 3-65, 3-66, and 3-67, respectively. The under relaxation factor α_R [-] is defined as 0.9 with unsteady particle tracking in transient flow simulation [26].

3.8 Summary

This chapter introduces the governing equations for the evaporation sub-model of a single droplet and the governing equations for the two-phase exchange. The results calculated by different evaporation models for defining the vapour-liquid equilibrium demonstrate a significant difference between the original model Raoult's law and the more accurate model UNIFAC. The adopted new model has been validated with experimental data [28]

Chapter 4. Evaporation process of a single droplet

Before modelling the spray's evaporation process, we should first focus on a single droplet's evaporation process applied to the Lagrangian model in spray modelling.

4.1 Two-component ethanol/iso-octane droplet evaporation

4.1.1 Model validation with existing numerical data

The evaporation of a single ethanol/iso-octane droplet in quiescent nitrogen is simulated using the 0-D (lumped) model introduced in chapter 2. The simulation validates the UNIFAC model and compares it with the existing numerical results [3]. The initial droplet diameter is 100μm [3], and the initial droplet temperature is $T_{d,0} = 25$ ℃ [3]. The ambient temperature and pressure are 600 ℃ and 10 bar, respectively [3], compared with published data. The initial fuel compositions are E36 and E78, i.e. the number stands for the volume fraction of ethanol in the mixture. The corresponding mole and mass fractions of ethanol in the E36 mixture are 61.3% and 39%, respectively. For E78, they are 90.83% and 80%, respectively. The results are calculated by both Raoult's and UNIFAC evaporation VLE models.

Time evolutions of the squared normalised droplet diameter $\frac{D_d^2}{D_{d,0}^2}$ and the droplet surface temperature $T_{d,s}$ are illustrated in Figures 4.1(a) and 4.1(b), respectively. The initial increase of the droplet diameter is caused by density reduction due to the rapid temperature rise of the droplet under heating, which overwhelms the impact of droplet mass loss due to

evaporation. The density properties for both components temperature-based variables and the density for each component is reducing throughout the whole evaporation process.

Three models (UNIFAC, NRTL, Raoult's) produce similar results except at the evaporation's final stage. For E36, the droplet lifetime calculated by the NRTL model is slightly longer than the other two models. For the E78 mixture, the droplet lifetime calculated by Raoult's law is slightly shorter than the other two models. The E78 (EM80) droplet has a slower evaporation process and thus a longer droplet lifetime than the E36 (EM39) one.

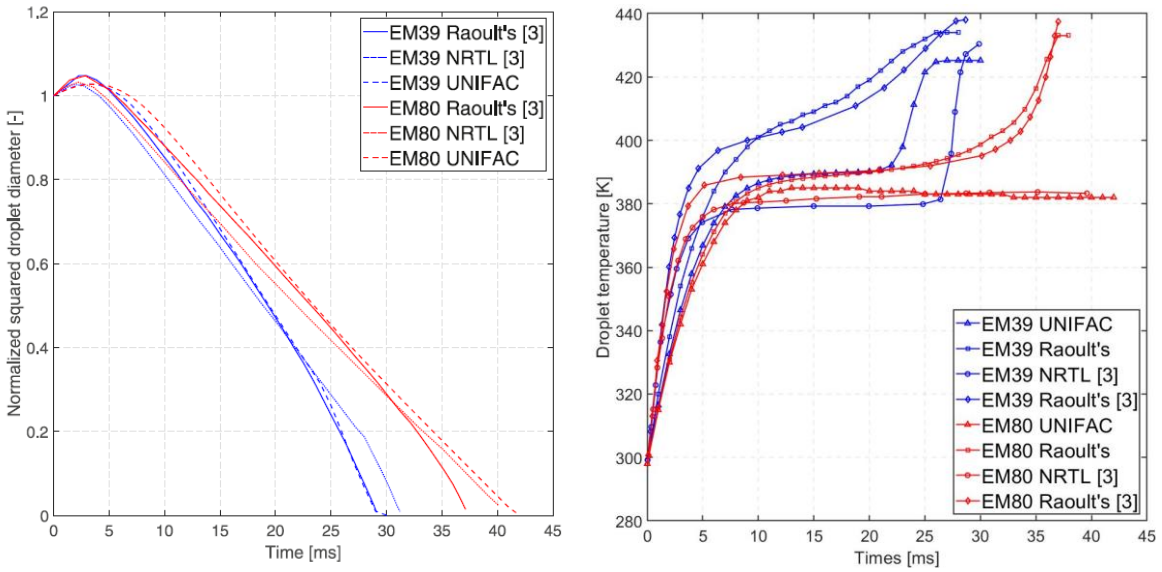

Figure 4.1 (a) droplet diameter (b) Droplet temperature

As shown in Fig. 4.1(b), the surface temperature of the E36 droplet calculated by Raoult's law monotonically increases with time, with a steeper and a smaller slope at the initial and later stages, respectively. Compared to Raoult's law, following an initial rapid increase in droplet temperature, a steady droplet temperature is reached with UNIFAC. Then a sharp rise in the droplet temperature is seen, which occurs at t = 24ms when ethanol in the droplet completes evaporation. NRTL in [3]

demonstrates a later time when both ethanol and iso-octane complete evaporation. For the E78 droplet, both UNIFAC and NRTL calculates the droplet temperature remains 380 K until the end of the droplet lifetime. With Raoult's law, the droplet temperature rapidly rises at the evaporation's final stage after t = 30 ms. The ratio between the iso-octane and ethanol mass of the droplet calculated by Raoult's law shows a sharp increase after 30 ms, as the minor component iso-octane is estimated to become the major component of the droplet gradually. With UNIFAC, the ratio decreases towards 0, i.e. ethanol is always the major component of the liquid mixture during the evaporation, and iso-octane completes evaporation first.

Liquid specific heat and Latent heat (enthalpy of vapourisation) are used to calculate the energy balance equation. The liquid specific heat is used to describe the energy needed to absorb to raise the liquid temperature. The latent heat is used to describe the energy required to evaporate the component from a liquid phase to the vapour phase. Figure 4.2 illustrates both component physical properties.

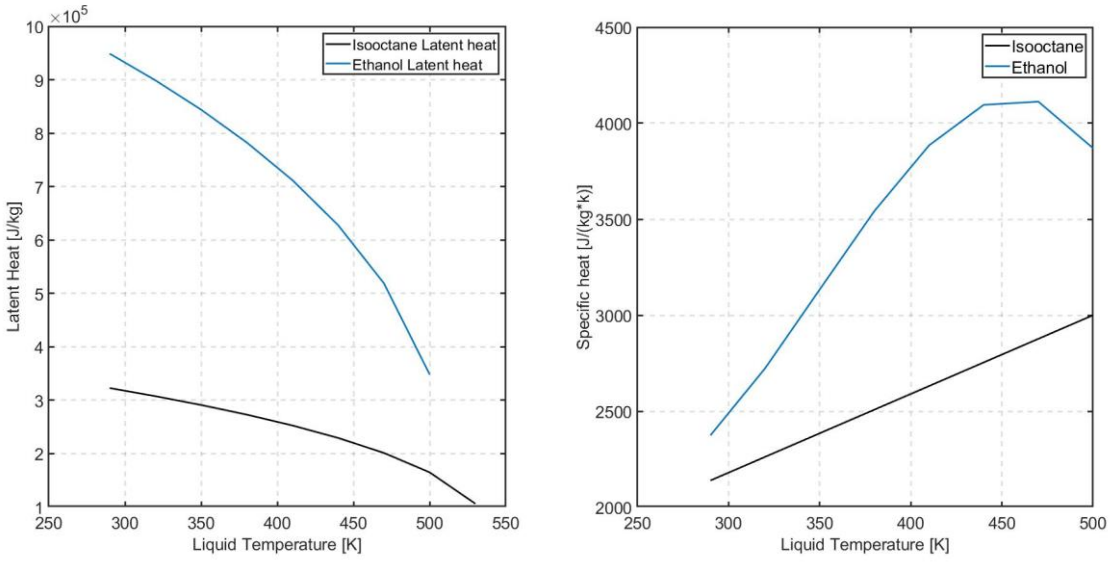

Figure 4.2. Latent heat (Left) and Specific heat (Right) of both components

The properties explain the sudden temperature rise in Figure 4.1 (b) as the ethanol has completed its evaporation shown in Figures 4.3 and 4.4. In figure 4.2, the latent heat of ethanol is much higher than the latent heat of Isooctane. For EM80 at approximate 35ms, the ethanol mass fraction calculated by Ideal Raoult's law has reduced to zero, which causes the sudden droplet temperature increase as isooctane does not need to absorb too much energy.

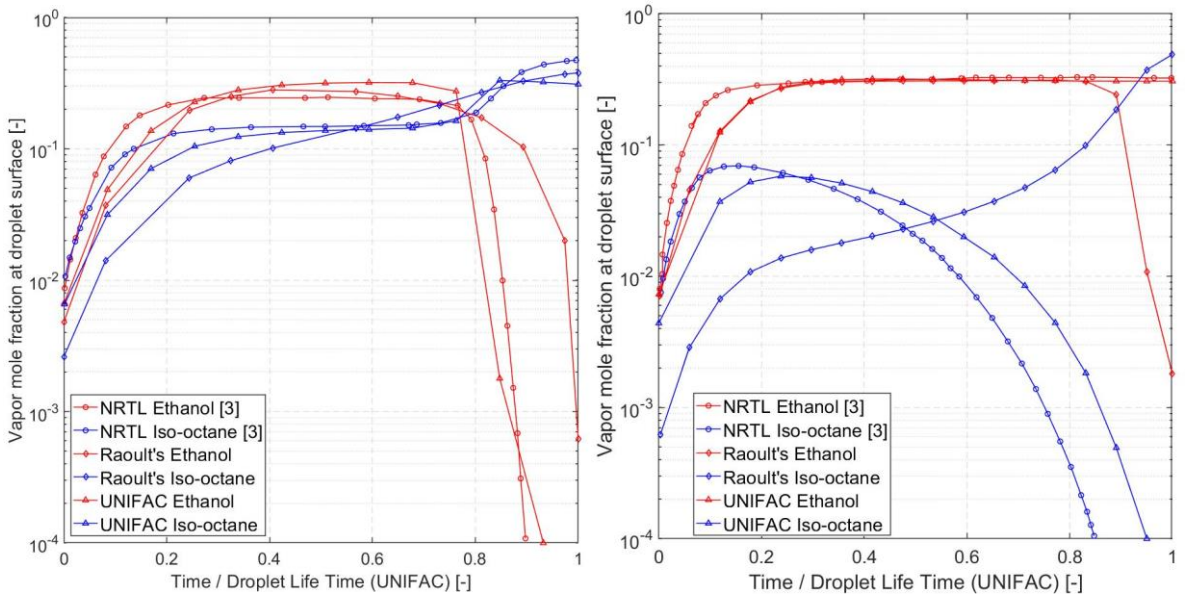

(a)E36/EM39 (b) E78/EM80

Figure 4.3. Vapour-phase mole fraction at the droplet surface.

A more detailed analysis based on vapour mole fractions $X_{i,v}$ at the droplet surface can further show the difference between an ideal and a more realistic VLE model. Figures 4.3(a) and 4.3(b) show $X_{i,v}$ of the E36 and E78 mixtures, respectively, in a 10-based logarithmic scale against a non-dimensional time normalised by the droplet lifetime. In Figure. 4(a), $X_{i,v}$'s of both components, ethanol (C2H5OH) and iso-octane(C8H18) calculated by the three models follow the same trends. Both $X_{C8H18,V}$ and $X_{C2H5OH,V}$ rapidly rise and then approaches an approximately steady value,

with a higher mole percentage of ethanol vapour at the droplet surface than iso-octane. At 80% of the droplet lifetime, the vapour mole fraction of the iso-octane rises again. The vapour mole fraction of the ethanol rapidly decreases towards 0 as the droplet evaporates completely. The UNIFAC and NRTL models produce very similar vapour mole fractions at the droplet surface during the whole course of the droplet evaporation. In contrast, the vapour phase mole fraction's quantitative results for Raoult's law is wrong, but the model calculates the right trend. The results from three VLE models indicate that Raoult's law can approximate the evaporation process of the E36 fuel evaporation.

However, the results for the E78 mixture simulated by three different models indicate otherwise. In Figure 4.3 (b), the vapour mole fraction of iso-octane calculated by both UNIFAC and NRTL models continuously decrease after an initial rise immediately after the droplet evaporation starts. The vapour mole fraction of iso-octane calculated by Raoult's Law monotonically increase during the evaporation. Besides, the mole fraction of ethanol calculated by Raoult's law rapidly decreases in the final stage. This trend does not exist in the evaporation processes calculated by both non-ideal models. The activity coefficients should be considered for this case to model the vapour-liquid equilibrium and droplet evaporation properly. Moreover, only compare the D^2 law is not sufficient to show that the droplet evaporation has been properly modelled, although the community has widely adopted this practice.

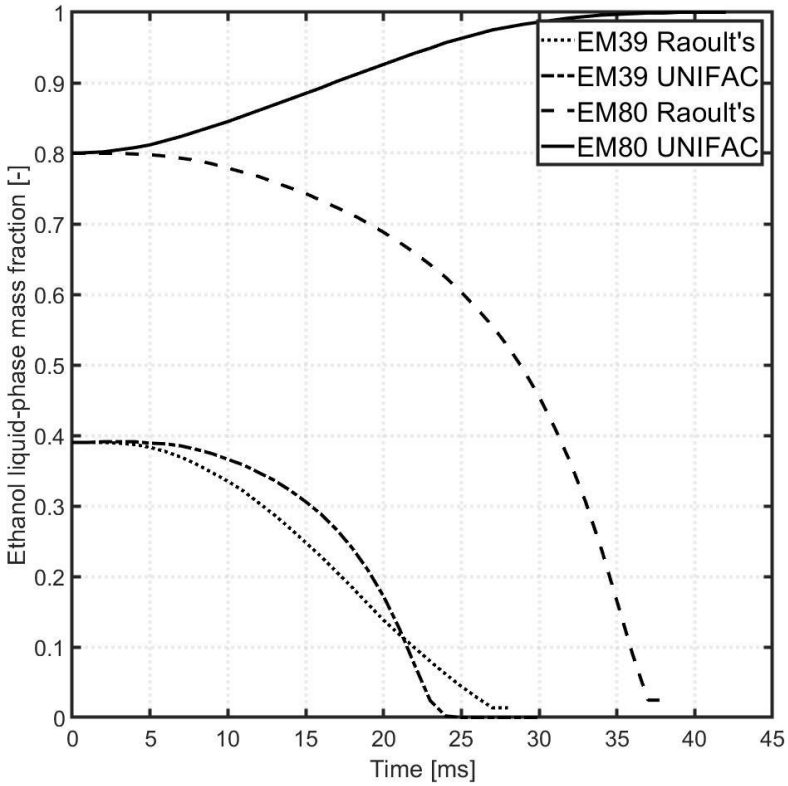

Figure 4.4. Liquid-phase mass fraction of ethanol

The liquid-phase mass fractions of ethanol in two cases (E36, E78) are shown in Fig. 4.4. Raoult's law can reasonably estimate the mass fraction of ethanol since the result demonstrates the same trend with the UNIFAC law. The mass fraction of ethanol calculated by UNIFAC law reduces more slowly at the early stage of the evaporation, and a steeper decrease at approximate 20ms is demonstrated in the Figure. In addition, the ethanol calculated by Raoult's law uses a longer time to evaporate.

On the other hand, the result for E78 demonstrates a different trend by using both the VLE model. Raoult's law provides a decreasing ethanol mass fraction, whereas UNIFAC shows an increasing mass fraction with evaporation time, indicating that the iso-octane component has a faster evaporation rate. The iso-octane completely evaporated at approximate 34ms for UNIFAC law.

A separation factor α_{ij} is introduced for measuring the relative volatility between two components i and j or which of the two components vaporises faster at the gas-liquid interface [3]. In the ideal VLE law (Raoult's law), α_{ij} depends only on saturation vapour pressures of pure components, i.e. $\alpha_{ij} = \frac{P_{sat,i}}{P_{sat,j}} = f(T)$, which is a function of temperature. Since saturation vapour pressure monotonically increases with temperature, α_{ij} will not undergo transition through 1 from less-than-1 to higher-than-1, the relative volatility of respective components in a mixture will remain identical to what the initial condition dictates throughout the evaporation process. For the more realistic VLE models, the separation factor is determined by a function of temperature, pressure and liquid-fuel composition. $\alpha_{ij} = \frac{\gamma_i P_{sat,i}}{\gamma_j P_{sat,j}} = f\left(T, X_{i,L}, P\right)$, which is a function of temperature, pressure and liquid-fuel composition.

The separation factor for E36 and E78 mixture is shown in Fig.4.5. It can be seen that for the E36 case, Raoult's law presents a correct trend of the relative volatility between the two components, although UNIFAC gives a lower separation factor throughout the droplet evaporation. While for the E78 case, since the separation factor throughout the droplet evaporation. While for the E78 case, since the separation factor calculated by Raoult's law depends exclusively on vapour pressure, the separation factor is very close to that for the E36 case. While for UNIFAC, $\alpha_{isooctane,ethanol}$ is very close to that for the E36 case. While for UNIFAC, $\alpha_{isooctane,ethanol} > 1$ even under the initial condition and during the whole evaporation process. In plain words, iso-octane is the more volatile component. It thus evaporates faster than ethanol in this case from the beginning of evaporation, despite a higher saturation vapour pressure of ethanol.

When a more “volatile” component, only in terms of saturation vapour pressure, is the major component of the liquid mixture, especially when its volume fraction is considerably higher than that of the liquid mixture, especially when its volume fraction is substantially higher than that of the other component, Raoult’s law will give misleading evaporation modelling results. With more realistic VLE models such as UNIFAC and NRTL taking into account the activity of the component and estimating a corrected liquid mole fraction by the activity coefficient γ_i, the separation factor can properly simulate the regime of the relative volatility between two components, which can be transited during or even from the beginning of the evaporation.

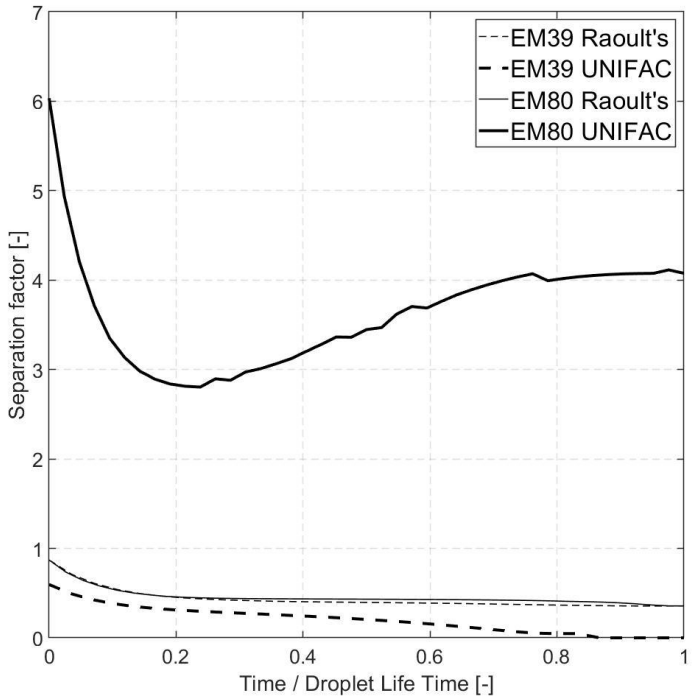

Figure 4.5. Separation factor during binary-component droplet evaporation, defined by the relative volatility of iso-octane compared to ethanol, i.e. if $\alpha_{isooctane,ethanol} > 1$, isooctane vaporises faster than ethanol.

4.1.2 Iso-octane/Ethanol droplet evaporation under different ambient conditions with the different initial composition

The single droplet study provides a fast and fundamental estimation of how the fuel mixture behaves inside the cylinder.

Three different combinations of iso-octane and ethanol are analysed with a mass fraction of 10% ethanol (EM10), 50% ethanol (EM50), 80% ethanol (EM80) to simulate the effect of droplet sizes and lifetime on the bi-component evaporation characteristics. The initial conditions for the droplet remain the same with an initial droplet diameter 100μm, and an initial droplet temperature 298K. Three different ambient pressure (5bar, 20bar, and 50bar) and three different ambient temperatures (473K, 673 K, and 873 K) are considered in the droplet simulation.

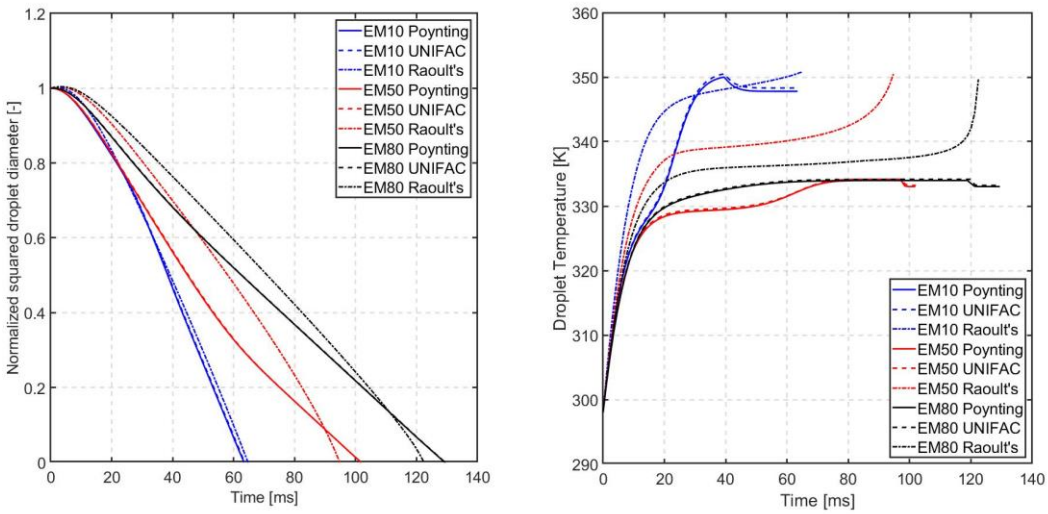

Figure4.6. droplet diameter (left) and droplet temperature (right) of 3 mixture combinations at 5bar, 473K

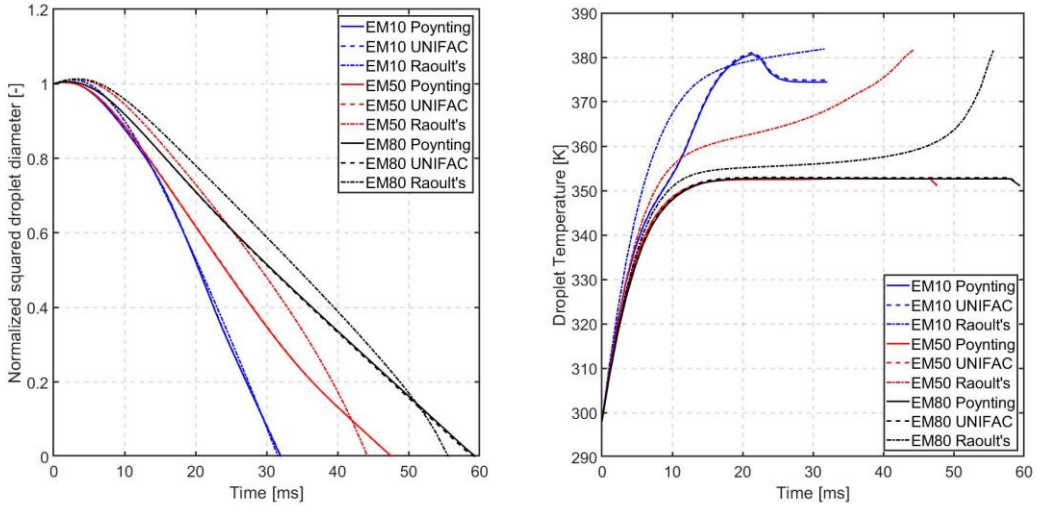

Figure 4.7. droplet diameter (left) and droplet temperature (right) of 3 mixture combination at 5bar, 673K

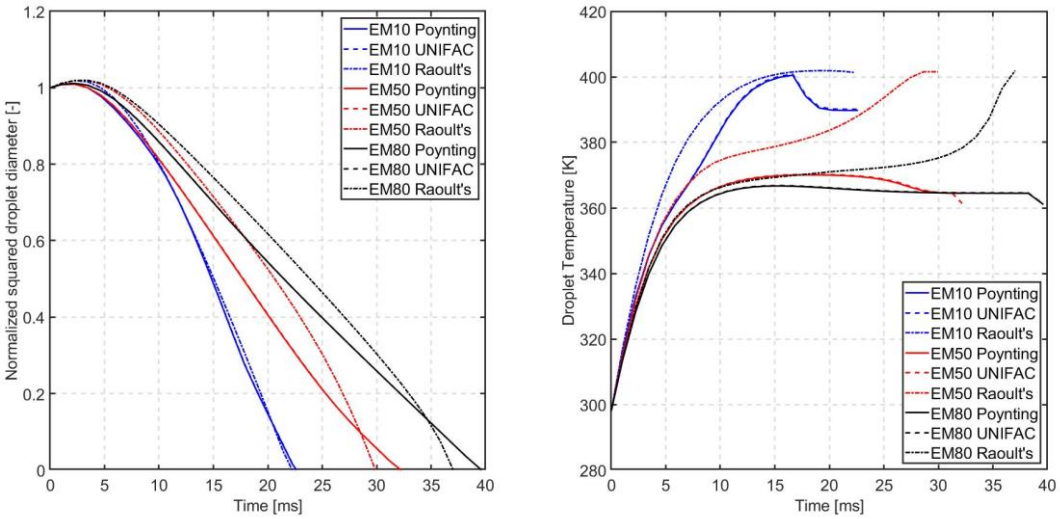

Figure 4.8. droplet diameter (left) and droplet temperature (right) of 3 mixture combinations at 5bar, 873K

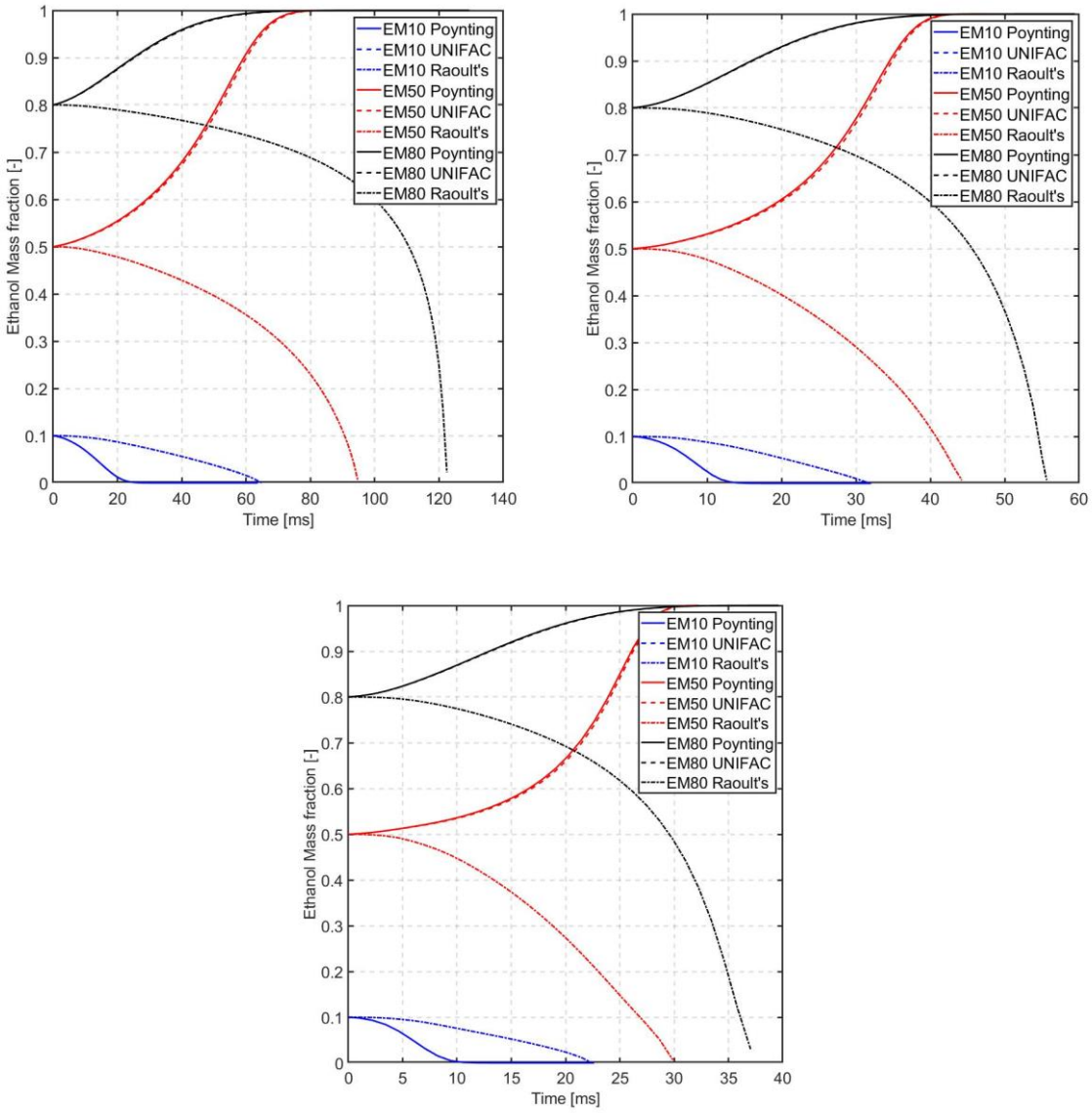

Figure 4.9. Ethanol mass fraction evolution at 5 bar (Top left 473K, Top right 673K, Bottom 873K)

Figure 4.5-4.8 illustrates the Bi-component droplet evaporation process with three different ambient temperatures with an ambient pressure at 5 bar. The droplet lifetime has significantly reduced with the increase of the ambient temperature. For EM80, the droplet lifetime is tripled as the ambient temperature is reduced. The overall droplet temperature also increased with the increased ambient temperature. The maximum droplet temperature has risen from 350 to 400K for the ideal VLE model. The

illustration for droplet temperature indicates that the ambient temperature significantly impacts droplet energy balance. The droplet absorbs more heat energy with an increased ambient temperature under the same ambient pressure. The Poynting factor has been introduced into the VLE model. However, at low ambient pressure 5 bar, the difference between the two models (Poynting Unifac and Unifac) is negligible. The difference between the Ideal VLE and Non-ideal VLE (Raoult's law and UNIFAC) cannot be ignored as all mixtures' results are wrong. The trends from EM10 are the same, but the ethanol evaporates much faster by applying the non-ideal models. The majority of the ethanol in the EM10 mixture has already evaporated at nearly one-third of the droplet lifetime for three different ambient temperatures. In contrast, the ethanol remains in the mixture at the end of the DLT by applying the ideal Raoult's law. In figure 4.9, On the other hand, the trends for both EM50 and EM80 are different as iso-octane evaporates faster than the ethanol and the ethanol mass fraction continuous to increase by applying the UNIFAC and Poynting UNIFAC models. The Ethanol is fully evaporated at the end of the DLT for both non-ideal models. The sudden temperature rise for EM50 and EM80 in figure 4.6 is due to the Ethanol component's total consumption.

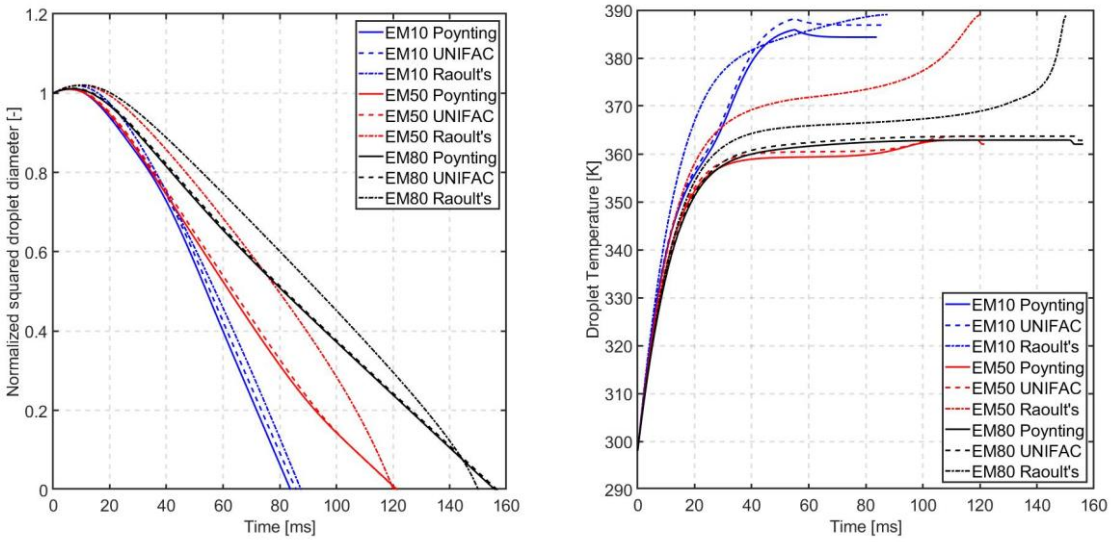

Figure 4.10. droplet diameter (left) and droplet temperature (right) of 3 mixture combinations at 20bar, 473K

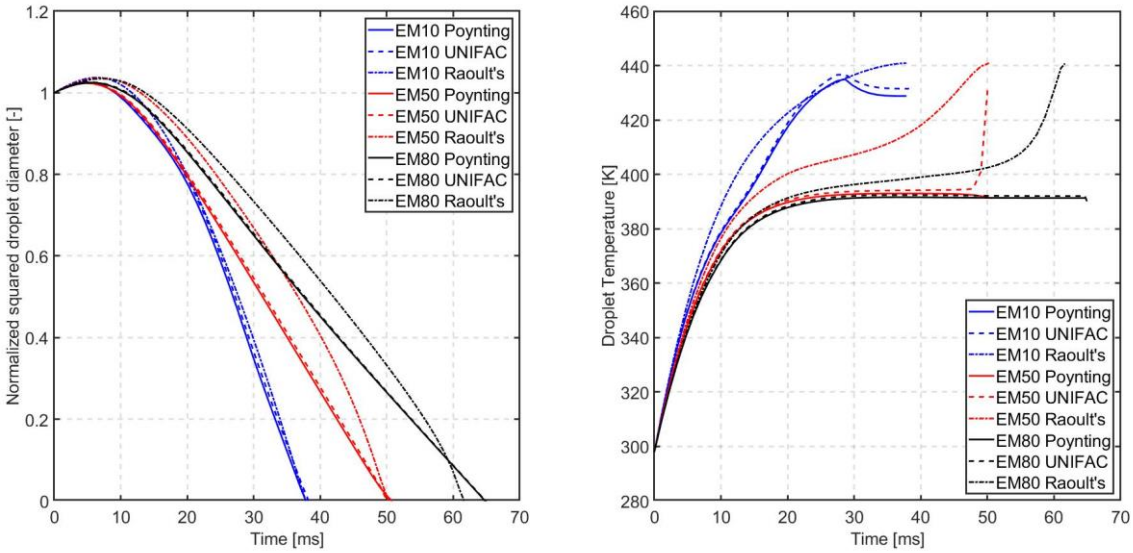

Figure 4.11. droplet diameter (left) and droplet temperature (right) of 3 mixture combination at 20bar, 673K

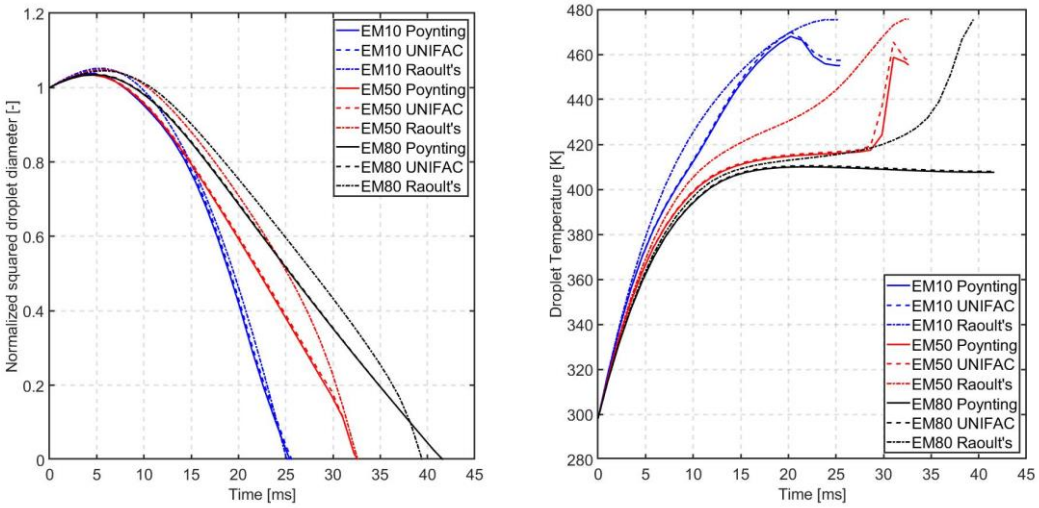

Figure 4.12. droplet diameter (left) and droplet temperature (right) of 3 mixture combinations at 20bar, 873K

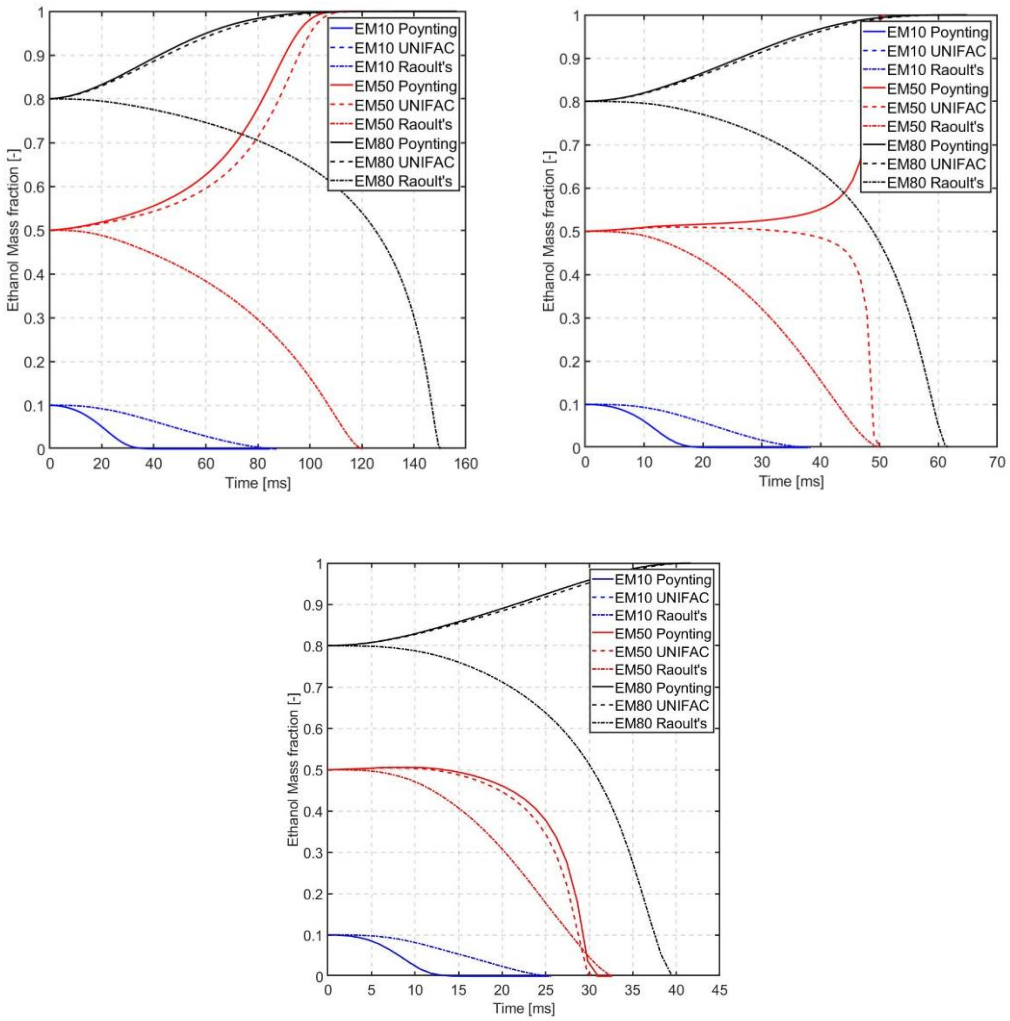

Figure 4.13. Ethanol mass fraction evolution at 20 bar (Top left 473K, Top right 673K, Bottom 873K)

Figure 4.10 to 4.13 illustrates the evaporation characteristics for three bi-components mixtures at three different ambient temperatures with an ambient pressure at 20 bar.

As the ambient pressure increased, the maximum droplet temperature during evaporation also increased, and the droplet lifetime also increased compared with a 5 bar ambient pressure shown in Figures 4.6 to 4.9. The EM10 and EM80 mixture demonstrates similar trends at 20 bar with the results at 5 bar. However, the Poynting factor has a significant impact at a higher ambient pressure. The results for EM50 at 473K demonstrates the same trends for all VLE models. The iso-octane is fully evaporated for both non-ideal models, whereas the ethanol evaporates faster and is fully consumed at the end by applying the ideal VLE model. What's more, the difference between the Poynting-UNIFAC model and the UNIFAC model becomes significant at 20 bar by simulating EM50 in Figure 4.13.

When the ambient temperature rose to 673 Kelvin at 20 bar, the results for EM50 changed dramatically as the Poynting UNIFAC model demonstrates different trends with UNIFAC and Raolt's model. The evolution of ethanol's mass fraction during evaporation presents the same results for UNIFAC and Raoult's law. However, the isooctane still primarily evaporated calculated by the Poynting-UNIFAC VLE model shown in Figure 4.13. Top right. At 873K with mixture EM50, all VLE models demonstrate the same trend, and the results are different from the EM50 results in Figure 4.9, where the ambient pressure is 5 bar.

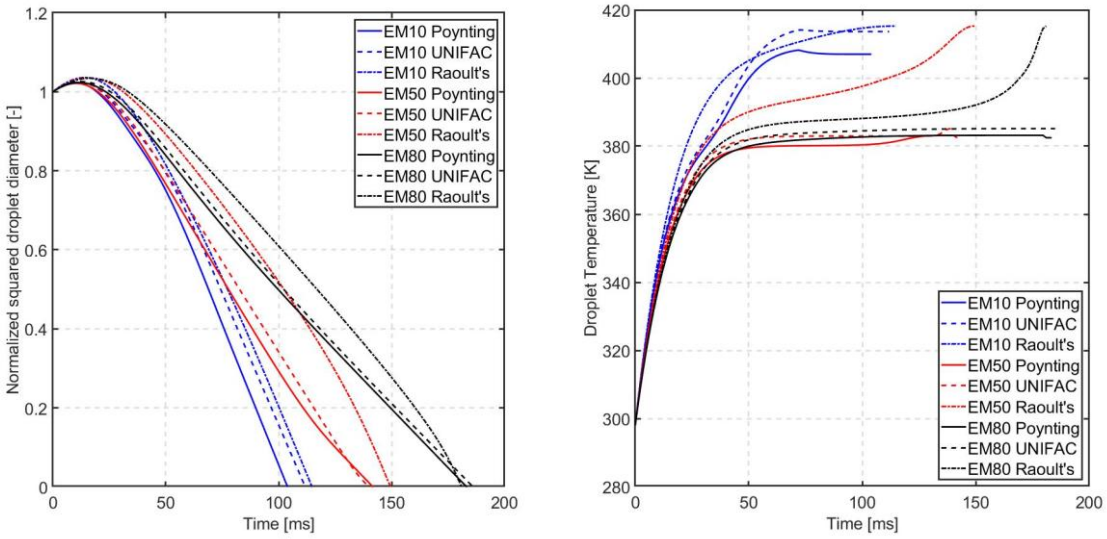

Figure 4.14. droplet diameter (left) and droplet temperature (right) of 3 mixture combination at 50bar, 473K

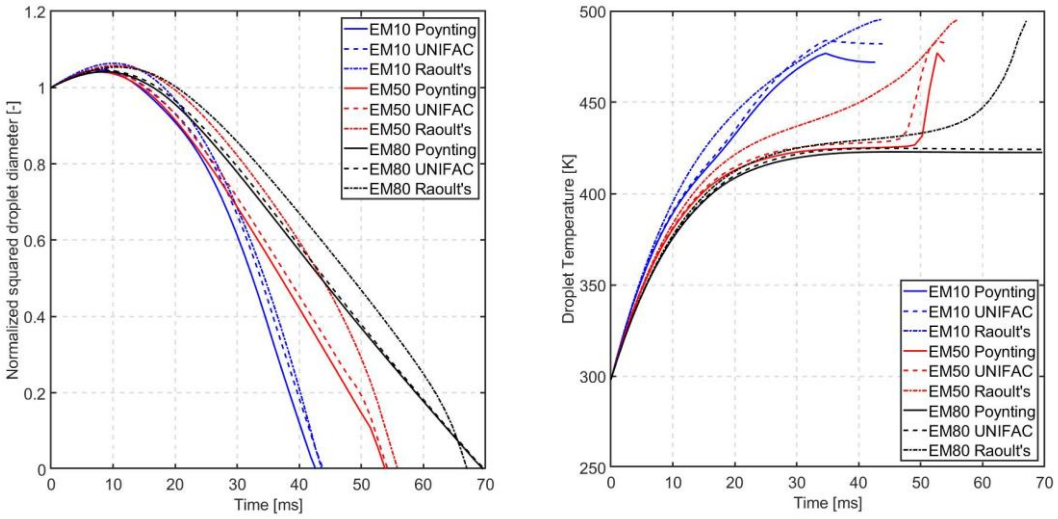

Figure 4.15. droplet diameter (left) and droplet temperature (right) of 3 mixture combination at 50bar, 673K

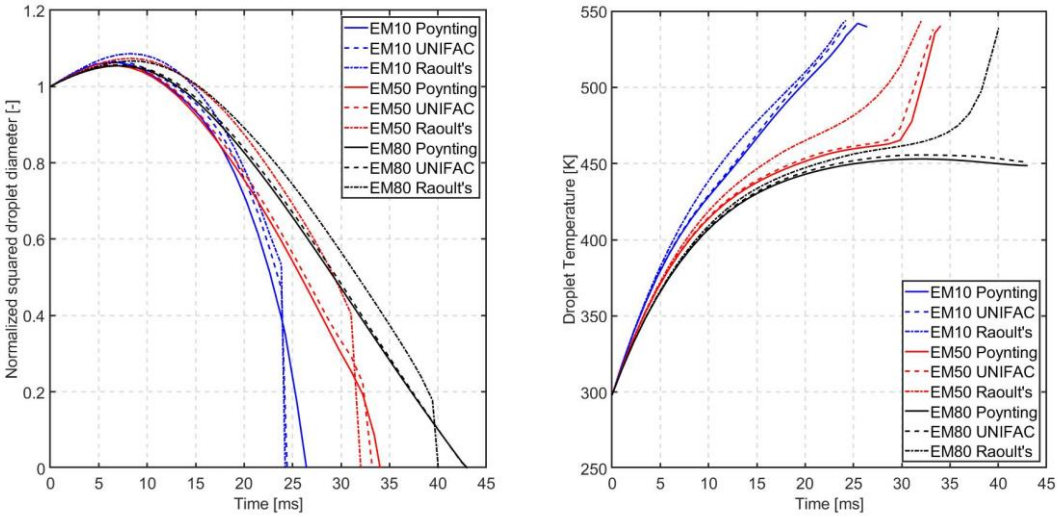

Figure 4.16. droplet diameter (left) and droplet temperature (right) of 3 mixture combinations at 50bar, 873K

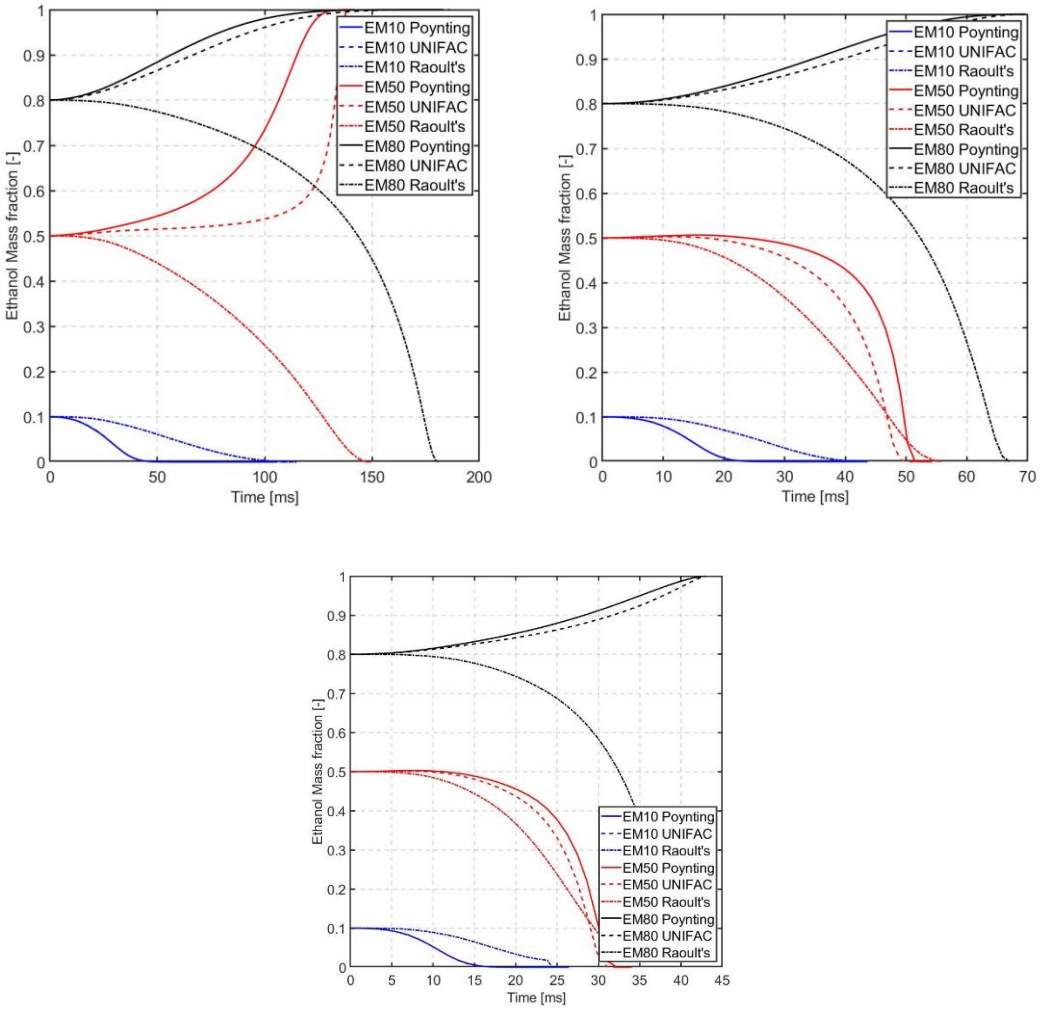

Figure 4.17. Ethanol mass fraction evolution at 50 bar (Top left 473K, Top right 673K, Bottom 873K)

Figure 4.14 to 4.17 illustrates the evaporation characteristics for three bi-components mixtures at three different ambient temperatures with an ambient pressure at 50 bar.

At 473 Kelvin, Both Poynting UNIFAC and UNIFAC models provide similar EM10 results in figure 4.17. And the droplet temperature evolution for EM10 is negligible. For EM50, the results for both non-ideal VLE models demonstrate the same trends in Figure 4.17. The droplet lifetime and temperature follow the same trend in Figure 4.14. In figure 4.16, the sudden sharp decrease of the EM10 droplet calculated by UNIFAC and Raoult's law is because the droplet reached the supercritical condition. All the liquid components will promptly alter to the gaseous phase. The critical temperature of iso-octane is 543.9 Kelvin, and the critical pressure of iso-octane is 26.5 bar. As the operating pressure is higher than the critical pressure, the evaporation law is no longer applicable when the droplet temperature reaches 543.9 K. The same situation also happens for the EM50 mixture calculated by Raoult's law. Therefore, the EM10 data will not use to compare with results under other operating conditions.

The EM80 mixture in all figures follows the same trend despite the ambient pressure and temperature. However, at a higher ambient pressure of 50 bar, compared with 20 bar and 5 bar, the results for EM80 calculated by Poynting UNIFAC and UNIFAC models have a noticeable difference shown in figure 4.16. The isooctane evaporates slightly faster, calculated by the Poynting UNIFAC compared with the UNIFAC model. The ethanol will always be the last component to evaporate for both non-ideal VLE models.

At 673k and 873k, the mass fraction evolution follows the trends of 873k at 20 bar, and all VLE models simulate the same trends for ethanol mass fraction.

Chapter 5 Multicomponent spray simulation

The VLE model has been implemented in ANSYS FLUENT. The liquid-phase here is solved by the ODE equation introduced in chapter 2: a 0-D, rapid internal mixing model is used to approximate the dispersing liquid phase by assuming all the liquid components are well mixed, and each droplet has a uniform temperature and species composition. The $k-\epsilon$ turbulence model is used to solve the turbulence kinetic energy k and the turbulent dissipation rate ϵ. No breakup models were considered.

The SIMPLE algorithm for pressure-velocity coupling is used. The least-squares cell-based method is used to compute spatial gradients, with a second-order scheme for pressure, second-order upwind schemes for momentum, component species and energy, first-order upwind schemes for k and ϵ, respectively. A first-order implicit scheme is used for time advancement for the transient simulation.

A single-hole simulation based on the study from P.Keller et al. [4] is presented using the developed numerical model. The experimental study was conducted in a constant volume chamber.

The three-dimensional simulation domain is $20 \times 20 \times 70 mm^3$ and filled with inert quiescent nitrogen initially. The ambient temperature and pressure are $T = 473K$ and $P = 0.56MPa$ [4], respectively. At the nozzle inlet, the injection pressure of the spray is $20MPa$ [4], the nozzle size provided by P.Keller et al. [4] is 115 micrometres. The injection velocity is $224m/s$ calculated by the Bernoulli equation, and the injection duration is $1ms$. The initial sizes of the injected Lagrangian parcels (sprayed droplets) follow a Rosin-Rammler distribution with a mean droplet size of $9\mu m$ [4].

The initial temperature of the discrete phase is $353K$. A pressure outlet with 0 turbulent intensity is used at the four side boundaries and the domain's downstream outlet. A cartesian mesh with a uniform grid spacing of 0.4mm in all three directions is used.

The above setup and initial/boundary conditions have been used for all spray simulations in the following sections.

5.1. Two-component ethanol/iso-octane sprays

The ethanol/iso-octane spray evaporation is simulated by using both VLE models. Two fuel compositions, i.e. E10 and E85, have been considered.

The ethanol vapour distributions for the E10 spray are shown in Fig.5.1. It can be seen that with Raoult's law, ethanol, as the more volatile component in the liquid mixture, is rapidly evaporated and produced immediately following the spray injection close to the nozzle. However, the ethanol, as the more volatile component in the liquid mixture, is rapidly evaporated and produced immediately following the spray injection close to the nozzle. However, the ethanol evaporation process calculated by UNIFAC law is even faster based on a higher activity coefficient of ethanol evaporation process calculated by UNIFAC law is even faster based on a higher activity coefficient of ethanol according to Fig.1. A line plot for the iso-octane vapour mass fraction $Y_{C_8H_{18},V}$ Calculated by Raoult's law, UNIFAC and NRTL at 30mm downstream of the nozzle are shown in Fig.5.2. There are no significant differences between the results from the three models. Raoult's law estimates slightly higher $Y_{C_8H_{18},V}$ on the spray jet centreline.

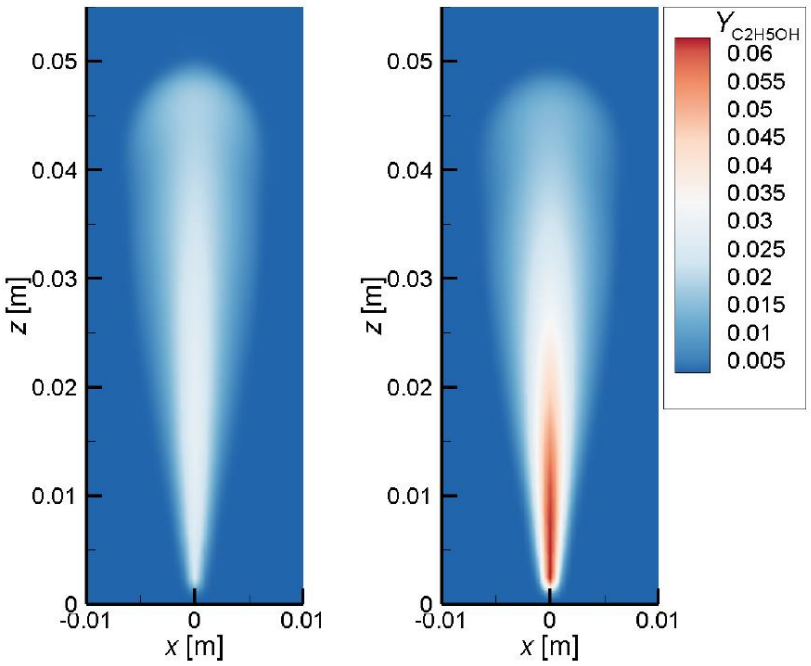

(a) Raoult's law (b) UNIFAC

Figure 5.1. Ethanol vapour distribution of an E10 spray at 1 ms

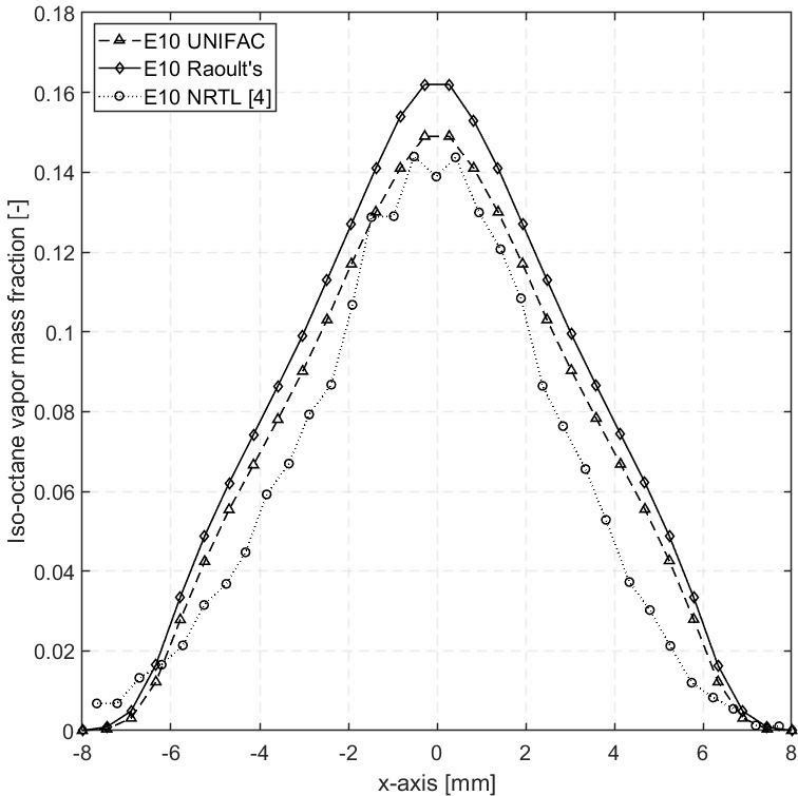

Figure 5.2. Isooctane vapour mass fraction $Y_{C_8H_{18},V}$ of an E10 spray at 30 mm downstream of the nozzle

For the E85 spray in which ethanol is the major component, the iso-octane vapour distribution at 1ms after the spray injection is shown in Fig. 5.3. Raoult's law estimates a much slower evaporation process of iso-octane and thus a much lower $Y_{C_8H_{18},V}$. At 30 mm downstream of the nozzle, $Y_{C_8H_{18},V}$ is slightly over 0.01 on the jet centreline with Raoult's law, but both UNIFAC and NRTL calculates $Y_{C_8H_{18},V} \approx 0.03$, as shown in Fig.4.4.

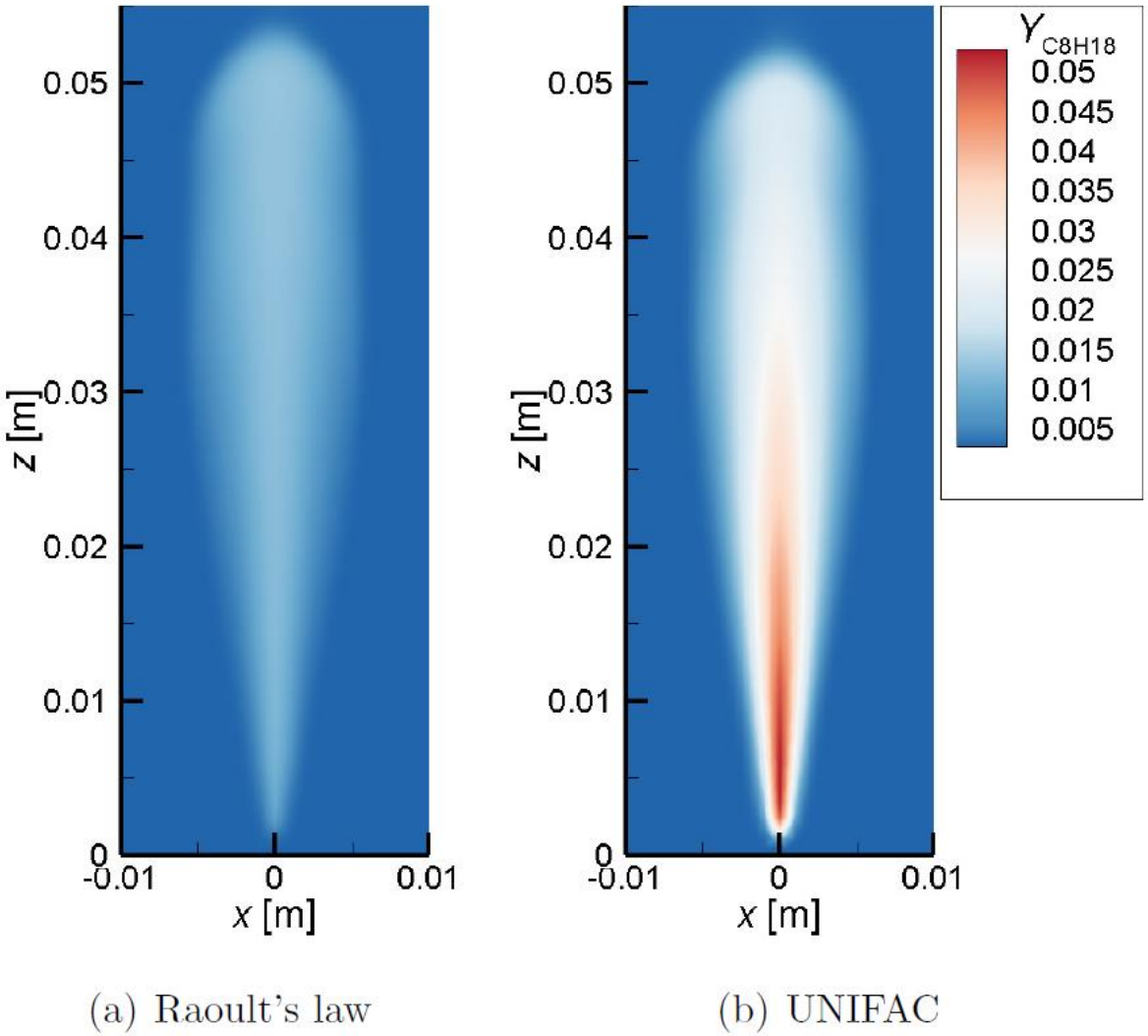

Figure 5.3. Isooctane vapour distribution of an E85 spray at 1ms.

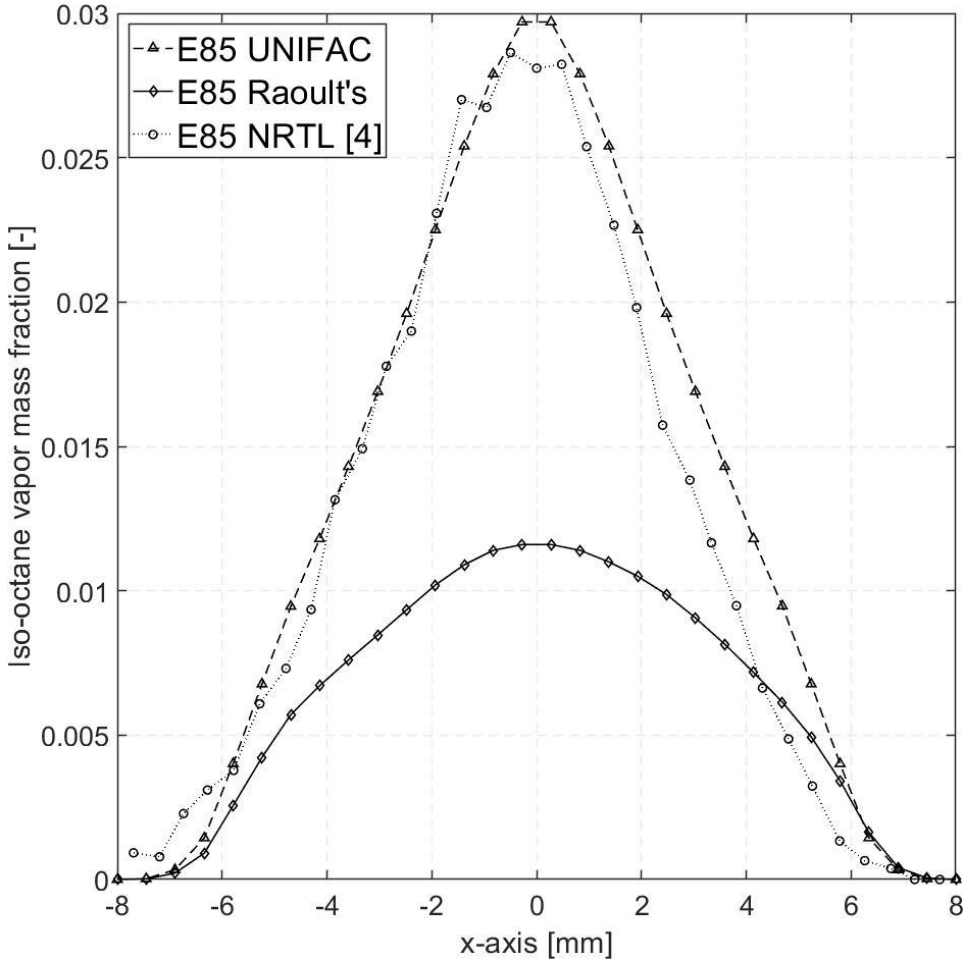

Figure 5.4. Isooctane vapour mass fraction $Y_{C_8H_{18},V}$ of an E85 spray at 30mm downstream of the nozzle.

5.2. Four-component gasoline/ethanol spray

Evaporation dynamics of a four-component gasoline/ethanol spray is simulated using Raoult's law and the UNIFAC model. A three-component mixture provided by FORD has been used as a surrogate for gasoline. The surrogate consists of n-pentane, iso-octane, and n-decane with a mass fraction of 0.24, 0.56 and 0.2, respectively. According to the distillation curve, the four-component fuel can achieve more realistic evaporation dynamics. An E85 spray is considered as the results demonstrates a significant deviation between the two VLE models.

Figure 5.5 illustrates the vapour mass fraction of n-pentane, iso-octane and ethanol along the spray jet centreline. Here decane is ignored as it

has little mass fraction and deviation calculated by both VLE models. Raoult's law demonstrates a rapid rise to a steady value of ~0.1 within a short distance at ~10% of the spray penetration length for the major component ethanol. However, with UNIFAC, the evaporation process of ethanol is much slower. The $Y_{C_2H_5OH,V}$ Slowly increases on the centreline towards the spray tip, where its maximal value below 0.07 is reached. The maximum value ethanol mass fraction calculated by the UNIFAC model is much lower than Raoult's law simulation.

For the major component iso-octane of the gasoline surrogate, the two VLE models' results are very different. The UNIFAC model illustrates a rapid growth of iso-octane mass fraction to its maximal value of 0.04 in the vicinity of the nozzle and slowly decreases towards the spray tip. However, the maximal mass fraction of iso-octane calculated by Raoult's law is less than 0.01, and the mass fraction continuously increases towards the spray tip. The n-pentane demonstrates a similar trend of its mass fraction towards the spray tip using two VLE models. But the maximum value is about twice the difference between the two models.

The vapour mass fraction of isooctane upstream near the nozzle is higher than that of ethanol calculated by the UNIFAC model, despite a much higher mass fraction of ethanol in the multicomponent liquid-fuel mixture. The results indicate the evaporation rate of isooctane is much higher than ethanol by using the UNIFAC model, whereas Raoult's calculated otherwise.

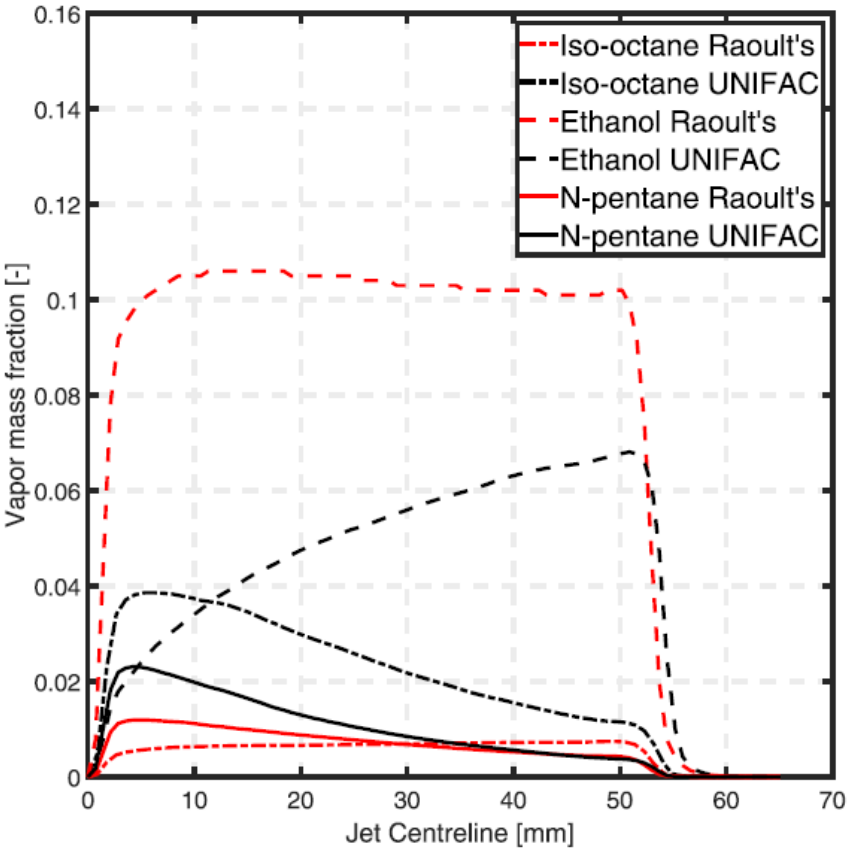

Figure 5.5. Vapour mass fraction of E85, four-component gasoline/ethanol spray at jet centreline.

Chapter 6. Conclusions and Future work

6.1 Novelty

Specific novel aspects of this research work are presented in this thesis:

The multi-component droplet evaporation models were created that accounted for non-ideal VLE. Both UNIFAC law and the Poynting factor are introduced into the Evaporation model. The models were deemed important due to the highly non-ideal nature of mixing between gasoline and alcohol-containing fuel blends.

Both droplet evaporation and spray evaporation are studied under different operating conditions. The spray simulation demonstrates the importance of using the NON-ideal models and explains the unexpected phenomena.

6.2 Conclusions

The in-cylinder fuel mixing process in a gasoline engine strongly influences the following combustion and emission formations. Due to the straightened emission regulations and increasing demand for the GDI engine, understanding the spray evaporation process is necessary.

The basic gasoline in markest includes E5, E15, commonly used in the EU and the USA. The oxygenated components such as ethanol and methanol are widely used in current gasoline engines to reduce engine emissions. The fuel blends should be simulated in a more detailed and

accurate model that requires the implementation of a non-ideal activity coefficient model.

Evaporation of a Bi-component ethanol/iso-octane droplet is firstly modelled and validated against published data. The results demonstrate that when component structures exhibit dissimilarity, the evaporation process calculated by the ideal VLE model can be misleading. For Raoult's law, the saturated vapour pressure of pure components affects the priority of vapour concentrations at the droplet surface for each component. However, a heavier component could evaporate faster than lighter components as the activity coefficient introduced in the VLE model. As shown in Both reference and the simulation, the heavier component iso-octane completes evaporation before the lighter component ethanol in the E78 mixture and EM80 mixture under all operating conditions.

The bi-component spray demonstrates significant deviations between two VLE models in spray simulation. The four-component n-pentane/isooctane/n-decane/ethanol spray shows a more significant difference at the spray jet centreline. The simulation for E85 spray at the downstream location is three times different between the UNIFAC model and Raoult's law.

6.3 Future work

6.3.1 Experimental studies on bi-component and multicomponent biofuel droplet

Most experimental studies only provide information on droplet temperature and size history, and the species evaporation rates are

normally ignored. The future research should include the evaporation rate of each component and the composition change during evaporation.

6.3.2 Combustion simulation for GDI spray with emission analysis

The stratified charge happened when the liquid fuel undertook an evaporation and mixing process. The vapour distribution calculated by both VLE models demonstrates a significant difference during the evaporation process. The combustion phenomenon can be completely different when the fuel and air are not fully premixed. The combustion simulation can enhance understanding the use of oxygenated fuel blends in GDI engines.

6.3.2 Multi-component mixtures

Current research works are based on a single component surrogate and a four-component surrogate. The surrogate can be extended to more complex multi-component fuel blends that provide a more detailed evaporation process and reaction phenomena.

Reference

[1] Robert H Perry and Don Green. Perry's Chemical Engineers' Handbook. New York: McGraw-Hill, 50thedition, 1984.

[2] IEA—International Energy Agency, 2011b. "Technology Roadmap, Biofuel for Transport". OECD/IEA, Paris. 2011

[3] A. Bader , P. Keller , C. Hasse , The influence of non-ideal vapor-liquid equi- librium on the evaporation of ethanol/iso-octane droplets, Int. J. Heat Mass Transf. 64 (2013) 547–558 .

[4] P. Keller , T. Knorsch , M. Wensing , C. Hasse , Experimental and numerical analysis of iso-octane/ethanol sprays under gasoline engine conditions, Int. J. Heat Mass Transf. 84 (2015) 497–510 .

[5] S. A. Morsi and A. J. Alexander. *"An Investigation of Particle Trajectories in Two-Phase Flow Systems"*. *J. Fluid Mech*. 55(2). 193–208. September 26 1972.

[6] R. D. Reitz. *"Mechanisms of Atomisation Processes in High-Pressure Vaporizing Sprays"*. *Atomisation and Spray Technology*. 3. 309–337. 1987.

[7] A. Daïf, M. Bouaziz, X. Chesneau, A. Ali Chérif, Comparison of multicomponent fuel droplet vaporization experiments in forced convection with the Sirignano model, Experimental Thermal and Fluid Science,Volume 18, Issue 4,1998,

[8] Frössling N. Über die Verdunstung fallender Tropfen. Gerlands Beitr. Geophys. 52: 170-216. 1938.

[9] Ranz WE and Marshall WR. Evaporation from Drops: Part I, Chemical Engineering Progress, 48 (3): 141-146. 1952.

[10] Beard KV and Pruppacher HR. A Wind Tunnel Investigation of the Rate of Evaporation of Small Water Drops Falling at Terminal Velocity in Air. J. Atmos.Sci, 1971 28: 1455-1465

[11] J. Tamim, W. Hallett, A continuous thermodynamics model for multicomponent droplet vaporisation, chem. Eng. Sci. 18(1995) 2933-2942.

[12] D. Ju, J. Xiao, Z. Geng, Z. Huang, Effect of mass fractions on evaporation of a multicomponent droplet at dimethyl ether (DME)/n-heptane-fueled engine conditions, Fuel 118 (2014) 227-237.

[13] D. Ju, T. Zhang, J. Jiao, X. Qiao, Z. Huang, Effect of droplet sizes on evaporation of a bi-component droplet at DME (dimethyl ether)/n-heptane-fueled engine conditions, Energy 86 (2015) 257-266.

[14] Y. Yu, S. Kang, Y. Kim and K.S. Lee, Numerical study on the characteristics of vaporisation, ignition and turbulent combustion processes in Dimethyl Ether (DME)-Fueled engine conditions, Energy & Fuels 2008, 22, 3649-3660.

[15] Lei. Zhang, S. Kong, Modeling of multicomponent fuel vaporisation and combustion for gasoline diesel spray, Chemical Engineering Science 64 (2009) 3688-3696.

[16] Y. Ra, RD. Reitz, A vaporisation model for discrete multicomponent fuel sprays, International Journal of Multiphase Flow 35 (2009) 101-117.

[17] X. Ren, L. Zhang&Z.Ji, simulation of diesel spray combustion using LES and a multicomponent vapourisation model, Combustion theory and modelling 2019 Vol.23, No. 1, 87-104.

[18] S. Sukumaran and S. Kong, Modelling biodiesel-diesel spray combustion using multicomponent vaporisation coupled with detailed fuel chemistry and soot models, Combustion theory and modelling 2016 Vol.20, No.5, 913-940.

[19] C.C. Wen, C.H. Tu, Vapor-liquid equilibria for binary and ternary mixtures of ethanol, 2-butanone, and 2,2,40trimethylpentane at 101.3 kPa, Fluid Ph. Equilibria 258 (2007) 131-139.

[20] P. Yi, W. Long, M. Jia, L. Feng, J. Tian, Development of an improved hybrid multicomponent vaporisation model for realistic multicomponent fuels, International Journal of Heat and mass transfer, 77(2014) 173-184.

[21] L. Zhang, S.C. Kong, Vaporisation modelling of petroleum-biofuel drops using a hybrid multicomponent approach, Combustion and Flame 157 (11) (2010) 2165-2174.

[22] L. Zhang, S.C. Kong, High-pressure vaporisation modelling of multicomponent petroleum-biofuel mixtures under engine conditions. Combustion and Flame 158 (9) (2011) 1705-1717.

[23] V. Ebrahimian, C. Habchi, Towards a predictive evaporation model for multicomponent hydrocarbon droplets at all pressure conditions, International journal of heat and mass transfer 54(2011) 3552-3565.

[24] P. Yi, W. Long, M. Jia, J. Tian, B. Li, Development of a quasi-dimensional vaporisation model for multicomponent fuels focusing on forced convection and high-temperature conditions. International journal of heat and mass transfer 97 (2016) 130-145.

[25] R.C. Reid , J.M. Prausnitz , B.E. Poling ,The Properties of Gases and Liquids, fourth ed., McGraw-Hill, London, 1987

[26] ANSYS, Inc. (2018) ANSYS Fluent User's Guide, Release 19.1

[27] P. Keller, T. Knorsch, M. Wensing and C. Hasse. The influence of differential evaporation on the structure of a three-component biofuel spray. International journal of engine research Vol. 16(5) 2015 610-626.

[28] K.H. Kwak, D. Jung and C. Borgnakke, Enhanced spray and evaporation model with multi-fuel mixtures for direct injection internal combustion engines, International of engine research 2014, Vol. 15(4) 488-503.

[29] M. Su, C.P. Chen. Heating and evaporation of a new gasoline surrogate fuel: A discrete multicomponent modelling study . Fuel 161 (2015) 215-221.

[30] C. Laurent, G. Lavergne, P. Villedieu. Quadrature method of momments for modelling multi-component spray vaporisation. International Journal of multiphase flow 36 (2010) 51-59.

[31] T. Kitano, J. Nishio, R. Kurose, S. Komori. Effects of ambient pressure, gas temperature and combustion reaction on droplet evaporation. Combustion and Flame 161(2014) 551-564.

[32] T. Kitano, J. Nishio, R. Kurose, S. Komori. Evaporation and combustion of multicomponent fuel droplets. Fuel 136(2014) 219-225.

[33] Software, R., Vectis Documentation Version 2015.2. 2015.

[34] X.Wang, and H. Zhao, "Numerical Simulation of the Gasoline Spray with an Outward-Opening Piezoelectric Injector: A Comparative Study of Different Breakup Models," SAE Technical Paper 2018-01-0272, 2018.

[35] A, Umemura. Turbulent atomization subgrid model for two-phase flow large eddy simulation (theoretical development). Combustion and Flame 165(2016) 154-176.

[36] Reitz, R.D. and Diwakar, R. " Structure of High-Pressure Fuel Sprays." SAE Paper 870598, SAE Transactions Vol. 96, Sect. 5, pp. 492-509, 1987.

[37] Liu, B, Mather, D., and Reitz, R. D., 1993, "Effects of Drop Drag and Breakup on Fuel Sprays," SAE Technical Paper No. 930072.

[38] Qian, J., Law, C.K., 1997. "Regimes of coalescence and separation in droplet collision". J. Fluid Mech. 331, 59–80.

[39] Brazier-Smith, P.R., Jennings, S.G., Latham, J., 1972. "The interaction of falling rain drops: coalescence". Proc. R. Soc. London, Ser. A 326, 393-408.

[40] Georjon, T.L., and Reitz, R.D. (1998). "A Drop Shattering Collision Model for MultiDimensional Spray Computations. Accepted for publication", Atomization and Sprays.

[41] Tennison, P.J., Georjon, T.L., Farrell, P.V. and Reitz, R.D. (1998). "An Experimental and Numerical Study of Sprays from a Common Rail Injection System for Use in an HSDI Diesel Engine". SAE Paper No. 980810.

[42] Post, S.L., Abraham, J., 2002. "Modeling the outcome of drop collisions in diesel sprays". Int. J. Multiphase Flow 28, 997-1019.

[43] Munnannur, A., & Reitz, R. D. (2007). "A new predictive model for fragmenting and on-fragmenting binary droplet collisions". International journal of multiphase flow, 33(8), 873-96.

[44] ML Greenfield, GA Lavoie, CS Smith, and EW Curtis. Macroscopic model of the D86 fuel volatility procedure. SAE Technical Paper 982724, 1998.

[45] Characteristics Study of DMF Using Phase Doppler Particle Analyzer," SAE Int. J. Passeng. Cars - Mech. Syst. 3(1): 948-958, 2010

[46] Christopher Price, Arash Hamzehloo, Pavlos Aleiferis, and David Richardson. Aspects of numerical modelling of flash-boiling fuel sprays. SAE Technical Paper 2015-24-2463, 2015.

[47] Xiao Hang Fang , Riyaz Ismail , Kendal Bushe & Martin Davy (2020) Simulation of ECN diesel spray A using conditional source-term estimation, Combustion Theory and Modelling, 24:4, 725-760

[48] Tanner, F.X., "Liquid Jet Atomization and Droplet Breakup Modeling of NonEvaporating Diesel Fuel Sprays," SAE Paper 970050, 1997.

[49] Ibrahim, E. A., Yang, H. Q., & Przekwas, A. J. (1993). "Modeling of spray droplets deformation and breakup". Journal of Propulsion and Power, 9(4), 651-654.

[50] Su, T. F., Patterson, M. A., Reitz, R. D., and Farrell, P. V., 1996, “Experimental and Numerical Studies of High Pressure Multiple-Injection Sprays,” SAE Technical Paper Series No. 960861.

[51] Tennison, P.J., Georjon, T.L., Farrell, P.V. and Reitz, R.D. (1998). "An Experimental and Numerical Study of Sprays from a Common Rail Injection System for Use in an HSDI Diesel Engine". SAE Paper No. 980810.

[52] Georjon, T.L., and Reitz, R.D. (1998). "A Drop Shattering Collision Model for MultiDimensional Spray Computations. Accepted for publication", Atomization and Sprays

[53] Ko, G.H., Ryou, H.S., 2005. "Modeling of droplet collision-induced breakup process". Int. J. Multiphase Flow 31, 723-738.

[54] W.P. Jones , V.N. Prasad , Large Eddy Simulation of the Sandia Flame Series D–F using the Eulerian stochastic field method, Combust. Flame 157 (9) (2010) 1621–1636 .

[55] V.M. Donell , M. Adachi , G.S. Samuelsen , Structure of reacting and nonreact- ing, non-swirling, air-assisted sprays, Part I: Gas-phase properties, Atomisation Sprays 3 (4) (1993) 389–410 .

[56] Faeth, G. M. (1983). "Evaporation and combustion of sprays". Progress in Energy and Combustion Science, 9(1), 1-76.

[57] Jin, J. and Borman, G., "A Model for Multicomponent Droplet Vaporization at High

Ambient Pressures," SAE Technical Paper 850264, 1985.

[58] Naber, J. and Reitz, R.D. (1988). "Modeling Engine Spray Wall Impingement". SAE Paper No. 880107.

[59] Zhong, S., Daniel, R., Xu, H., Zhang, J., Turner, D. and Wyszynski, M.L., "Combustion and emissions of 2, 5-Dimethylfuran in a direct-injection spark-ignition engine," Energy Fuels, 24 (2010), pp. 2891–2899.

[60] Tian, G., Li, H., Xu, H., Li, Y., & Satish, M. R. (2010). "Spray characteristics study of DMF using phase doppler particle analyzer. SAE International Journal of Passenger Cars-Mechanical Systems, 3(1), 948-958

[61] Godsave, G. A. E., 1953, “Studies of the Combustion of Drops in a Fuel Spray—The Burning of Single Drops of Fuel,” Fourth Symposium International on Combustion, Williams and Wilkins, Baltimore, pp. 818–830.

[62] Kong S.C., Han Z., and Reitz, R.D. “The Development and Application of a Diesel Ignition and Combustion Model for Multidimensional Engine Simulation”, SAE paper 950278, 1995.

[63] de Villiers, E., Gosman, A., and Weller, H., "Large Eddy Simulation of Primary Diesel Spray Atomization," SAE Technical Paper 2004-01-0100, 2004

[64] Arcoumanis, C. and Gavaises, M.. “Linking nozzle flow with spray characteristics in a diesel fuel injection system”. Atomization and Sprays 8.3 (1998) 307–347.

[65] Nishimura, A., Assanis, D.N., "A Model for Primary Diesel Fuel Atomization Based on Cavitation Bubble Collapse Energy", 8th Int. Conf. on Liquid Atomization and Spray Systems, Pasadena, pp.1249-1256, 2000.

[66] Jenny, P., Roekaerts, D., & Beishuizen, N. (2012). "Modeling of turbulent dilute spray combustion". Progress in Energy and Combustion Science.

[67] V. Vuorinen, A. Wehrfritz, C. Duwig, B.J. Boersma, Large-eddy simulation on the effect of injection pressure and density on fuel jet mixing in gas engines, Fuel 130 (2014) 241–250, doi: 10.1016/j.fuel.2014.04.045

[68] A. Wehrfritz, V. Vuorinen, O. Kaario, M. Larmi, Large eddy simulation of high-velocity fuel sprays: studying mesh resolution and breakup model effects for Spray A, At. Sprays 23 (5) (2013) 419–442

[69] J. Benajes, R. Payri, M. Bardi, P. Martí-Aldaraví, Experimental characterization of diesel ignition and lift-offlength using a single-hole ECN injector, Appl. Ther- mal Eng. 58 (1–2) (2013) 554–563

[70] L.M. Pickett, D.L. Siebers, Soot in diesel fuel jets: effects of ambient tem- perature, ambient density, and injection pressure, Combust. Flame 138 (1–2) (2004) 114–135

[71] S.S. Sazhin. Modelling of fuel droplet heating and evaporation: Recent results and unsolved problems. Fuel 196 (2017) 69-101.

[72] Suzzi, D. (2009). "Diesel nozzle flow and spray formation: coupled simulations with real engine validation".

[73] G. Brenn , L.J. Deviprasath , F. Durst , C. Fink , Evaporation of acoustically lev-itated multi-component liquid droplets, Int. J. Heat Mass Transf. 50 (2007) 5073–5086

[74] Tuckermann R, Bauerecker S, and Neidhart B. Evaporation rates of alkanes and alkanols from acoustically levitated droplets, Analytical and Bioanalytical Chemistry, (2002) 372 (1): 122-127.

[75] Roth N and Frohn A. Measuring technique to investigate the evaporation process of droplets consisting of hydrocarbon mixtures. Proc. of the 13th Int. Conf. on Liquid Atomisation and Spray Systems, Florence, Italy.

[76] T. Knorsch, M.Heldmann, L. Zigan, M. Wensing, A. Leipertz. On the role of physicochemical properties on evaporation behavior of DISI biofuel spray. Exp Fluids (2013) 54:1522

[77] Mats Andersson, Jonas Warnberg, Stina Hemdal, Petter Dahlander and Ingemar Denbratt. Evaporation of Gasoline-like and Ethanol-Based Fuels in Hollow-Cone Sprays Investigated by Planar Laser-Induced Fluorescence and Mie Scattering. SAE 2011-01-1889.

[78] S.S. Sazhin, Advanced models of fuel droplet heating and evaporation, Prog. Energy Combust. Sci. 32 (2006) 162-214.

[79] C, L, Yaws. Thermophysical properties of chemicals and hydrocarbons

[80] Reitz, R. D. "Atomization and other breakup regimes of a liquid jet." 1978.